PLOS BIOLOGY

RESEARCH ARTICLE

Autophagy prevents early proinflammatory responses and neutrophil recruitment during *Mycobacterium tuberculosis* infection without affecting pathogen burden in macrophages

Rachel L. Kinsella*, Jacqueline M. Kimmey¤, Asya Smirnov, Reilly Woodson, Margaret R. Gaggioli, Sthefany M. Chavez, Darren Kreamalmeyer, Christina L. Stallings*

Department of Molecular Microbiology, Center for Women's Infectious Disease Research, Washington University School of Medicine, St. Louis, Missouri, United States of America

¤ Current address: Department of Microbiology and Environmental Toxicology, UC Santa Cruz, Santa Cruz, California, United States of America
* rlkinsella@wustl.edu (RLK); stallings@wustl.edu (CLS)

Citation: Kinsella RL, Kimmey JM, Smirnov A, Woodson R, Gaggioli MR, Chavez SM, et al. (2023) Autophagy prevents early proinflammatory responses and neutrophil recruitment during *Mycobacterium tuberculosis* infection without affecting pathogen burden in macrophages. PLoS Biol 21(6): e3002159. https://doi.org/10.1371/journal.pbio.3002159

Academic Editor: Hans-Uwe Simon, University of Bern, SWITZERLAND

Received: April 12, 2023

Accepted: May 11, 2023

Published: June 15, 2023

Data Availability Statement: All relevant data are within the paper and its Supporting Information files.

Funding: This work was supported by NIH grants R01 AI132697 and U19 AI142784, a Burroughs Wellcome Fund Investigators in the Pathogenesis of Infectious Disease Award (1016714), and the Philip and Sima Needleman Center for Autophagy Therapeutics and Research to C.L.S., a Potts

Abstract

The immune response to *Mycobacterium tuberculosis* infection determines tuberculosis disease outcomes, yet we have an incomplete understanding of what immune factors contribute to a protective immune response. Neutrophilic inflammation has been associated with poor disease prognosis in humans and in animal models during *M. tuberculosis* infection and, therefore, must be tightly regulated. ATG5 is an essential autophagy protein that is required in innate immune cells to control neutrophil-dominated inflammation and promote survival during *M. tuberculosis* infection; however, the mechanistic basis for how ATG5 regulates neutrophil recruitment is unknown. To interrogate what innate immune cells require ATG5 to control neutrophil recruitment during *M. tuberculosis* infection, we used different mouse strains that conditionally delete *Atg5* in specific cell types. We found that ATG5 is required in $CD11c^+$ cells (lung macrophages and dendritic cells) to control the production of proinflammatory cytokines and chemokines during *M. tuberculosis* infection, which would otherwise promote neutrophil recruitment. This role for ATG5 is autophagy dependent, but independent of mitophagy, LC3-associated phagocytosis, and inflammasome activation, which are the most well-characterized ways that autophagy proteins regulate inflammation. In addition to the increased proinflammatory cytokine production from macrophages during *M. tuberculosis* infection, loss of ATG5 in innate immune cells also results in an early induction of T_H17 responses. Despite prior published in vitro cell culture experiments supporting a role for autophagy in controlling *M. tuberculosis* replication in macrophages, the effects of autophagy on inflammatory responses occur without changes in *M. tuberculosis* burden in macrophages. These findings reveal new roles for autophagy proteins in lung resident macrophages and dendritic cells that are required to suppress inflammatory responses that are associated with poor control of *M. tuberculosis* infection.

Memorial Foundation postdoctoral fellowship to R. L.K., and a National Science Foundation Graduate Research Fellowship DGE-1143954 and the NIGMS Cell and Molecular Biology Training Grant GM007067 to J.M.K. The funders had no role in study design, data collection and analysis, decision to publish, or preparation of the manuscript. None of the authors received a salary from any of the funders.

Competing interests: The authors have declared that no competing interest exist.

Abbreviations: BMDM, bone marrow-derived macrophage; DC, dendritic cell; dpi, days postinfection; hpi, hours postinfection; LAP, LC3-associated phagocytosis; ROS, reactive oxygen species; TB, tuberculosis; WT, wild-type.

Introduction

According to the World Health Organization, 10 million people fell ill with *Mycobacterium tuberculosis* infection and 1.5 million people died of tuberculosis (TB) in 2020, marking the first increase in TB-associated deaths in over a decade [1]. Whether a person controls the initial *M. tuberculosis* infection or develops active TB disease is directly impacted by the type of immune response elicited in the infected individual [2]. Therefore, better understanding of what constitutes a protective versus non-protective immune response to *M. tuberculosis* infection is critical for developing better therapies and prevention measures to fight this deadly disease. Genetic mouse models have provided invaluable insight into the immunological processes that are required for control of *M. tuberculosis* infection. Infection of mice through the aerosol route leads to phagocytosis of *M. tuberculosis* by alveolar macrophages, initiating an inflammatory response and recruitment of innate immune cells to the lung [2]. *M. tuberculosis* replicates within these innate immune cells until antigen specific T cells traffic to the lung where they activate the innate immune cells to restrain *M. tuberculosis* replication and suppress inflammation. *M. tuberculosis* establishes a chronic infection in wild-type (WT) mice, which survive for over a year with this infection.

Atg5$^{fl/fl}$*-LysM-Cre* mice, which delete the *Atg5* gene specifically in macrophages, inflammatory monocytes, some dendritic cells (DCs), and neutrophils, are severely susceptible to *M. tuberculosis* infection [3–5], highlighting ATG5 as a critical component of a protective immune response to *M. tuberculosis*. *M. tuberculosis*-infected *Atg5*$^{fl/fl}$*-LysM-Cre* mice fail to control bacterial replication and succumb to infection by 40 days postinfection (dpi) [3–5]. The uncontrolled *M. tuberculosis* replication is associated with an early (by 14 dpi) and sustained influx of neutrophils in the *M. tuberculosis*-infected *Atg5*$^{fl/fl}$*-LysM-Cre* mice. Depletion of neutrophils during *M. tuberculosis* infection in *Atg5*$^{fl/fl}$*-LysM-Cre* mice rescues the susceptibility and extends their survival [3], demonstrating that the neutrophil-dominated inflammation contributed to their susceptibility. In general, higher abundance of neutrophils during *M. tuberculosis* infection have been associated with worse disease outcomes in mice [6–13] and humans [12,14–17]. Therefore, understanding the regulatory mechanisms that govern neutrophil recruitment and accumulation during *M. tuberculosis* infection could be key for manipulating inflammatory responses to better control TB.

ATG5 is required for the intracellular pathway of autophagy, a process by which cytoplasmic contents are targeted to the lysosome for degradation [18,19]. Initiation of autophagy involves phagophore formation from the endoplasmic reticulum, which is mediated by the ULK1 complex (ULK1/ULK2, ATG13, FIP200, and ATG101) and the PI3 kinase complex (ATG14L, BECLIN1, VPS15, and VPS34) [20,21]. Elongation of the autophagosomal double membrane depends on 2 ubiquitin-like conjugation systems. In the first system, ATG12 is activated by ATG7, transferred to ATG10, and covalently attached to ATG5. The second ubiquitin-like component is LC3 (microtubule-associated protein 1 light chain 3), which is conjugated to phosphatidylethanolamine, generating the membrane bound form called LC3-II through the actions of ATG7 and ATG3. ATG5-ATG12 facilitates LC3 lipidation through its interactions with ATG3, while ATG16L1 specifies the localization of LC3 conjugation to the autophagosome membrane [18,19,21,22]. The autophagosome membrane is then completed and targeted for fusion with the lysosome where the autophagosome cargo are degraded. In addition, ATG5 also functions outside of autophagy, including during *M. tuberculosis* infection [3], although these activities remain poorly understood. Recent work supports an autophagy-dependent role for ATG5 in LysM^{+} innate immune cells in suppressing neutrophil recruitment to the lungs during *M. tuberculosis* infection [23]. Using in vitro cell culture experiments, multiple groups have reported that macrophages require autophagy to control *M.*

tuberculosis replication by targeting the pathogen to the lysosome (xenophagy) as well as to prevent necrosis following days of infection in culture [5,23–29]. However, to date there is no evidence that xenophagy functions in this capacity in vivo. Therefore, the mechanistic basis for how loss of ATG5 results in early and exaggerated recruitment of neutrophils during *M. tuberculosis* infection in vivo remains unknown.

In this manuscript, we dissect the role for ATG5 in regulating neutrophil recruitment and accumulation during *M. tuberculosis* infection in vivo. We find that ATG5 functions with other autophagy proteins specifically in $CD11c^+$ lung macrophages and DCs to limit the production of cytokines and chemokines that otherwise promote neutrophil influx to the lung early in *M. tuberculosis* infection. We demonstrate that loss of autophagy in macrophages and DCs does not affect *M. tuberculosis* burden in these cell types in vivo and instead changes the inflammatory response to the infection. In addition, ATG5 is required in lung macrophages and DCs to limit IL-17A production from $CD4^+$ T cells. Together, our studies reveal new roles for ATG5 and other autophagy proteins in regulating inflammatory responses during infection, which with further dissection could provide insight into pathways that may be targeted to effectively promote protective immune responses during TB.

Results

ATG5 is required in $CD11c^+$ lung macrophages and DCs to control neutrophil recruitment and accumulation early during *M. tuberculosis* infection in vivo

M. tuberculosis infection of *Atg5$^{fl/fl}$-LysM-Cre* mice results in the recruitment of a higher number of neutrophils in the lungs at 14 dpi as compared to *Atg5$^{fl/fl}$* controls, despite equivalent bacterial burdens at this time point [3]. There are also no differences in the abundance of non-neutrophil cell types in *Atg5$^{fl/fl}$-LysM-Cre* and *Atg5$^{fl/fl}$* mice at 14 dpi [3]. This indicates that specifically neutrophils are accumulating in *M. tuberculosis*-infected *Atg5$^{fl/fl}$-LysM-Cre* mice due to a defect in inflammatory responses to infection and not due to higher burden. To determine which $LysM^+$ cells required ATG5 to control the early influx of neutrophils into the lungs during *M. tuberculosis* infection, we compared bacterial burdens and neutrophil inflammation in *Atg5$^{fl/fl}$-LysM-Cre*, *Atg5$^{fl/fl}$-Mrp8-Cre* (deletion in neutrophils), *Atg5$^{fl/fl}$-Cd11c-Cre* (deletion in lung macrophages and DCs), and *Atg5$^{fl/fl}$* controls at 14 dpi. At 14 dpi, the *Atg5$^{fl/fl}$-LysM-Cre* and *Atg5$^{fl/fl}$-Cd11c-Cre* mice, but not *Atg5$^{fl/fl}$-Mrp8-Cre* mice, had higher levels of neutrophil inflammation in the lungs as compared to *Atg5$^{fl/fl}$* controls (**Fig 1A and 1B**). The degree of increased neutrophil frequency was similar in *Atg5$^{fl/fl}$-LysM-Cre* and *Atg5$^{fl/fl}$-Cd11c-Cre* mice, indicating that loss of *Atg5* in $CD11c^+$ cells, but not neutrophils, leads to the early influx of neutrophils into the lungs during *M. tuberculosis* infection. At 14 dpi, none of the mouse strains harbored increased *M. tuberculosis* burden in their lungs (**Fig 1C**), indicating that the increase in neutrophil abundance in *Atg5$^{fl/fl}$-Cd11c-Cre* mice is not due to elevated bacterial burden and reflects a dysregulated inflammatory response to infection.

To determine if the higher levels of neutrophils in the lungs of *M. tuberculosis*-infected *Atg5$^{fl/fl}$-CD11c-Cre* mice was due to elevated neutrophil abundance in circulation prior to or during infection, we monitored neutrophil frequency in the blood in uninfected and 14 dpi *Atg5$^{fl/fl}$* and *Atg5$^{fl/fl}$-CD11c-Cre* mice. There was no significant difference in the frequency of neutrophils in the blood of uninfected or 14 dpi *Atg5$^{fl/fl}$* and *Atg5$^{fl/fl}$-CD11c-Cre* mice (**S1A Fig**), suggesting that the accumulation of neutrophils in the lungs of *M. tuberculosis*-infected *Atg5$^{fl/fl}$-CD11c-Cre* mice was due to specific recruitment of neutrophils to the site of infection or an inability to clear neutrophils from the lung. To begin to investigate this latter possibility, we monitored whether dead neutrophils were accumulating in the lungs of *Atg5$^{fl/fl}$-CD11c-Cre*

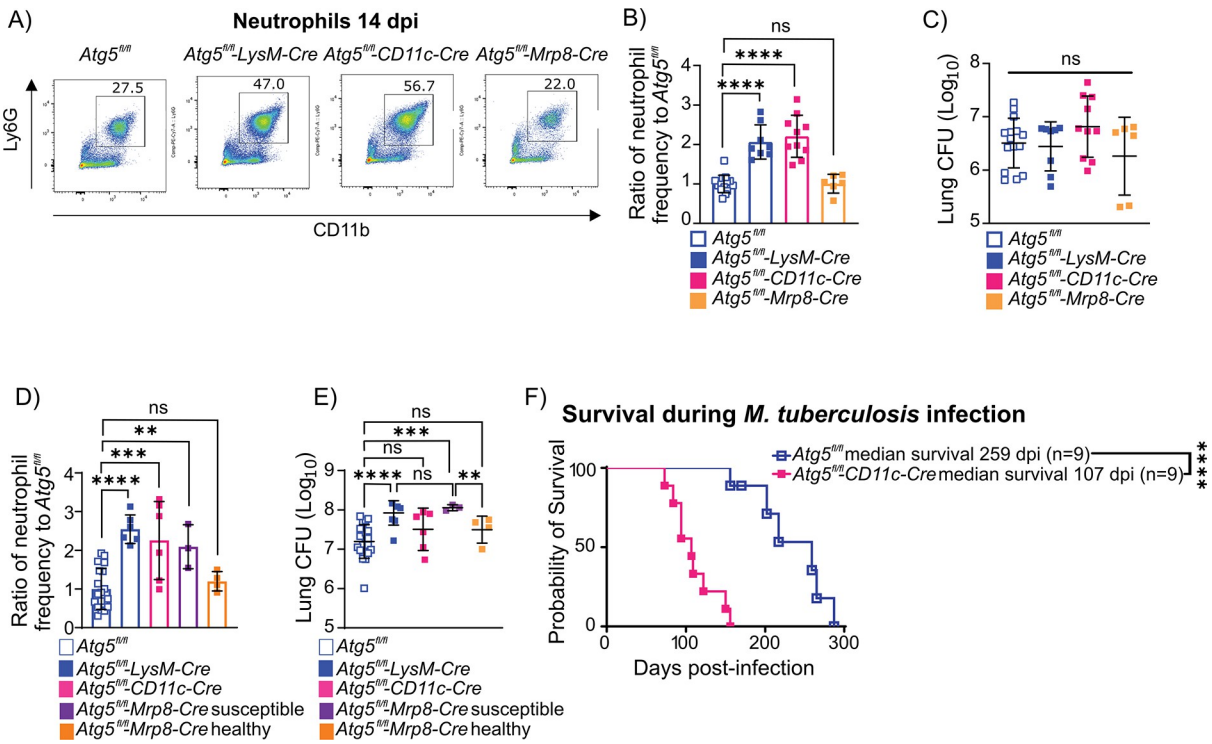

Fig 1. ATG5 is required in CD11c^{+} cells to regulate the early influx of neutrophils during *M. tuberculosis* infection in vivo. (A) Representative flow cytometry plots of neutrophils (CD45^{+}Ly6G^{+}CD11b^{+}) at 14 dpi from *Atg5$^{fl/fl}$*, *Atg5$^{fl/fl}$-LysM-Cre*, *Atg5$^{fl/fl}$-CD11c-Cre*, and *Atg5$^{fl/fl}$-Mrp8-Cre* mice. **(B)** Proportion of CD45^{+} cells that are neutrophils in the lung at 14 dpi in *Mtb*-GFP infected *Atg5$^{fl/fl}$* ($n = 15$), *Atg5$^{fl/fl}$-LysM-Cre* ($n = 8$), *Atg5$^{fl/fl}$-CD11c-Cre* ($n = 10$), and *Atg5$^{fl/fl}$-Mrp8-Cre* ($n = 6$) mice. Neutrophil frequency is reported as a ratio relative to the average neutrophil frequency in *Atg5$^{fl/fl}$* control mice at 14 dpi within a given experiment. **(C)** Lung burden from the right lung at 14 dpi in *Mtb*-GFP infected *Atg5$^{fl/fl}$* ($n = 15$), *Atg5$^{fl/fl}$-LysM-Cre* ($n = 8$), *Atg5$^{fl/fl}$-CD11c-Cre* ($n = 10$), and *Atg5$^{fl/fl}$-Mrp8-Cre* ($n = 6$) mice. **(D)** Proportion of CD45^{+} cells that are neutrophils in the lung at 21 dpi in *Mtb*-GFP infected *Atg5$^{fl/fl}$* ($n = 19$), *Atg5$^{fl/fl}$-LysM-Cre* ($n = 6$), *Atg5$^{fl/fl}$-CD11c-Cre* ($n = 6$), and *Atg5$^{fl/fl}$-Mrp8-Cre* ($n = 7$) mice. Neutrophil frequency is reported as a ratio relative to the average neutrophil frequency in *Atg5$^{fl/fl}$* control mice at 21 dpi within a given experiment. Susceptible and healthy *Atg5$^{fl/fl}$-Mrp8-Cre* mice are defined as done previously where susceptible *Atg5$^{fl/fl}$-Mrp8-Cre* mice have lost more than 5% of their pre-infection body weight by 20 dpi and healthy *Atg5$^{fl/fl}$-Mrp8-Cre* mice have lost less than 5% of their pre-infection body weight at 20 dpi [3]. **(E)** Lung burden from the right lung at 21 dpi in *Mtb*-GFP infected *Atg5$^{fl/fl}$* ($n = 19$), *Atg5$^{fl/fl}$-LysM-Cre* ($n = 6$), *Atg5$^{fl/fl}$-CD11c-Cre* ($n = 6$), and *Atg5$^{fl/fl}$-Mrp8-Cre* ($n = 7$) mice. **(F)** Kaplan–Meier curve of survival proportions during *Mtb*-GFP infection of *Atg5$^{fl/fl}$* ($n = 9$) and *Atg5$^{fl/fl}$-CD11c-Cre* ($n = 9$) mice. Statistical differences were determined by a log-rank Mantel–Cox test (F) or one-way ANOVA and Šídák multiple comparison test (B–E). * $P < 0.05$, ** $P < 0.01$, *** $P < 0.001$, **** $P < 0.0001$. Differences that are not statistically significant are designated as ns. Pooled data from at least 2 separate experiments is graphed where each data point is from 1 biological replicate. The individual numerical values used to generate the graphed data in **Fig 1**, the statistical analyses performed to analyze these data, and the *p* values from these statistical tests are in **S1 Data.** dpi, days postinfection.

https://doi.org/10.1371/journal.pbio.3002159.g001

mice during *M. tuberculosis* infection by analyzing neutrophil viability at 14 dpi by flow cytometry (**S1B Fig**). We did not observe a significant difference in the frequency of viable neutrophils at 14 dpi in *Atg5$^{fl/fl}$* and *Atg5$^{fl/fl}$-CD11c-Cre* mice, indicating that increased neutrophil inflammation in the lungs of *Atg5$^{fl/fl}$-CD11c-Cre* mice was not due to differences in neutrophil viability.

The higher levels of neutrophils in the lungs of *Atg5$^{fl/fl}$-LysM-Cre* and *Atg5$^{fl/fl}$-Cd11c-Cre* mice were sustained through 21 dpi (**Fig 1D**). However, only *Atg5$^{fl/fl}$-LysM-Cre* mice, and not *Atg5$^{fl/fl}$-Cd11c-Cre* mice, had higher bacterial burdens in the lungs at 21 dpi (**Fig 1E**), similar to as previously reported [3]. Loss of *Atg5* in neutrophils results in increased susceptibility to *M. tuberculosis* infection in some, but not all, *Atg5$^{fl/fl}$-Mrp8-Cre* mice [3]. The susceptible *Atg5$^{fl/fl}$-Mrp8-Cre* mice accumulate higher neutrophil numbers and bacterial burdens in their lungs at 21 dpi (**Fig 1D and 1E**) [3]. Therefore, loss of *Atg5* in neutrophils is likely contributing

to the higher burdens in the lungs of *Atg5*$^{fl/fl}$*-LysM-Cre* mice at 21 dpi. These data indicate that ATG5 has a role in CD11c^{+} lung macrophages and DCs to regulate early recruitment of neutrophils, but not the control of *M. tuberculosis* replication during *M. tuberculosis* infection at 14 and 21 dpi.

To determine how the loss of Atg5 in CD11c^{+} cells and the resulting early influx of neutrophils into the lungs affected host susceptibility, we monitored survival in *M. tuberculosis*-infected *Atg5*$^{fl/fl}$*-Cd11c-Cre* mice as compared to *Atg5*$^{fl/fl}$ controls. *Atg5*$^{fl/fl}$*-Cd11c-Cre* mice succumbed to *M. tuberculosis* infection between 100 and 150 dpi, which was significantly earlier than *Atg5*$^{fl/fl}$ controls (median survival time of 259 dpi) (**Fig 1F**), but not as early as *Atg5*$^{fl/fl}$*-LysM-Cre* mice (succumb 30 to 40 dpi [3]). These data demonstrate that ATG5 is required in CD11c^{+} lung macrophages and DCs to control early neutrophil recruitment and promote survival following *M. tuberculosis* infection.

The role for ATG5 in lung macrophages and DCs in regulating neutrophil recruitment is dependent on other autophagy proteins

Deletion of multiple different autophagy genes in all LysM^{+} innate immune cells can result in increased neutrophil recruitment to the lung during *M. tuberculosis* infection [23]. However, we previously showed that at least 1 role for ATG5 in LysM^{+} innate immune cells in controlling *M. tuberculosis* infection is autophagy independent [3]. Therefore, it is not known if the role for ATG5 specifically in CD11c^{+} lung macrophages and DCs is the same as described when broadly deleting *Atg5* in all LysM^{+} cells. To determine whether the regulation of neutrophil recruitment by ATG5 in CD11c^{+} lung macrophages and DCs was dependent on other autophagy proteins or represented the autophagy-independent role for ATG5 during *M. tuberculosis* infection, we monitored neutrophil abundance in the lungs of mice lacking expression of another essential autophagy protein, BECLIN 1, in CD11c^{+} cells (*Becn1*$^{fl/fl}$*-Cd11c-Cre*) at 14 dpi by flow cytometry. Similar to *Atg5*$^{fl/fl}$*-Cd11c-Cre* mice, *Becn1*$^{fl/fl}$*-Cd11c-Cre* mice also exhibited elevated neutrophil frequency in the lung at 14 dpi relative to *Becn1*$^{fl/fl}$ control mice (**Fig 2A**), despite no difference in bacterial burden (**Fig 2B**). In addition, analysis of *M. tuberculosis*-infected *Atg16l1*$^{fl/fl}$*-LysM-Cre* and *Becn1*$^{fl/fl}$*-LysM-Cre* mice also revealed higher levels of neutrophils in the lungs at 14 dpi relative to controls, without higher bacterial burdens (**Fig 2C and 2D**).

In addition to their role in canonical autophagy, the proteins ATG5, BECLIN 1, and ATG16L1 are also required for the process of LC3-associated phagocytosis (LAP), where LC3 is recruited to the phagosome, resulting in LC3^{+} single membrane vesicles that traffic to the lysosome for degradation. LAP can dampen inflammatory responses through efferocytosis, pathogen removal, stimulating inhibitory immune-receptor signaling, and reducing auto-antigen levels [30–33]. In contrast to canonical autophagy, LAP uses RUBICON and UVRAG instead of ATG14 in the PI3K complex and does not depend on ULK1 [33,34]. To distinguish between whether ATG5, BECLIN 1, and ATG16L1 were functioning through autophagy or LAP to regulate neutrophil recruitment during *M. tuberculosis* infection, we infected mice lacking RUBICON expression, a protein specifically required for LAP. *Rubicon*$^{-/-}$ mice had no difference in neutrophil accumulation or bacterial burdens as compared to WT controls following *M. tuberculosis* infection (**Fig 2C and 2D**), indicating that LAP is not required to control neutrophil inflammation during *M. tuberculosis* infection. Importantly, BECLIN 1 and ATG5 function at different steps of autophagy. Therefore, the requirement of both BECLIN 1 and ATG5 suggests that both the initiation and elongation steps of autophagy are required in CD11c^{+} cells to control neutrophil recruitment early during *M. tuberculosis* infection. Targeting of pathogens to the lysosome via autophagy is termed xenophagy, and multiple studies

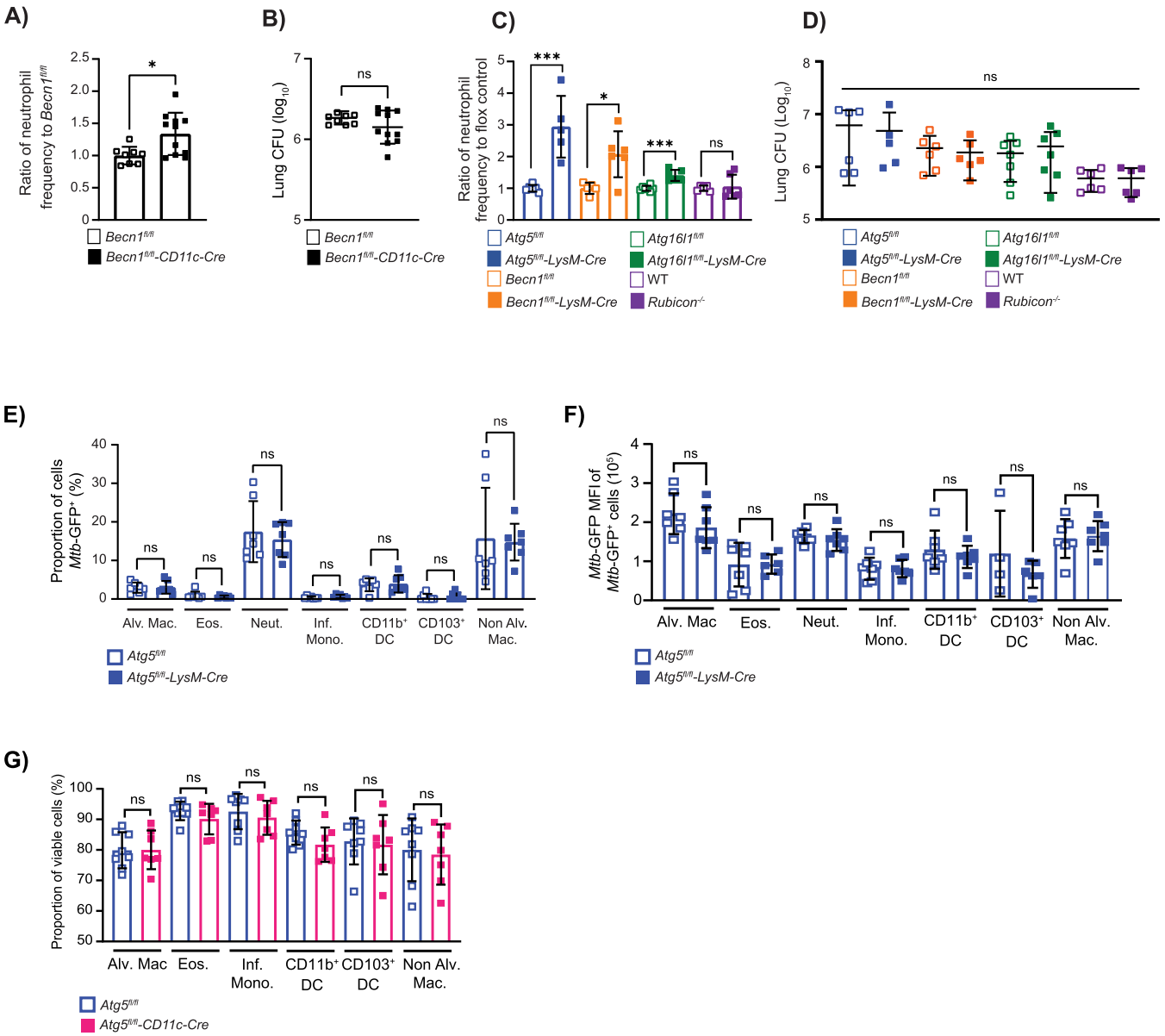

Fig 2. The role for ATG5 in lung macrophages and DCs in regulating neutrophil recruitment is dependent on other autophagy proteins but does not involve control of pathogen infection or burden. (A) Proportion of $CD45^+$ cells that are neutrophils ($CD45^+Ly6G^+CD11b^+$) in the lung at 14 dpi in *Mtb*-GFP infected *Becn1*$^{fl/fl}$ ($n = 8$) or *Becn1*$^{fl/fl}$*-CD11c-Cre* ($n = 11$) mice. Neutrophil frequency is reported as a ratio relative to the average neutrophil frequency in *Becn1*$^{fl/fl}$ control mice at 14 dpi. **(B)** Lung burden from the right lobes of the lung at 14 dpi in *Mtb*-GFP infected *Becn1*$^{fl/fl}$ ($n = 8$) or *Becn1*$^{fl/fl}$*-CD11c-Cre* ($n = 11$) mice. **(C)** Neutrophil frequency of $CD45^+$ cells reported as a ratio to the average neutrophil frequency in floxed control mice at 14 dpi in *Mtb*-GFP infected *Atg5*$^{fl/fl}$ ($n = 6$), *Atg5*$^{fl/fl}$*-LysM-Cre* ($n = 5$), *Becn1*$^{fl/fl}$ ($n = 6$), *Becn1*$^{fl/fl}$*-LysM-Cre* ($n = 6$), *Atg16l1*$^{fl/fl}$ ($n = 7$), and *Atg16l1*$^{fl/fl}$*-LysM-Cre* ($n = 7$) mice. Neutrophil frequencies at 14 dpi in *Mtb*-GFP infected *Rubicon*$^{-/-}$ ($n = 6$) mice were compared to WT C57BL/6J ($n = 6$) mice. **(D)** Lung burden from right lobes of the lung at 14 dpi in *Mtb*-GFP infected *Atg5*$^{fl/fl}$ ($n = 6$), *Atg5*$^{fl/fl}$*-LysM-Cre* ($n = 5$), *Becn1*$^{fl/fl}$ ($n = 6$), *Becn1*$^{fl/fl}$*-LysM-Cre* ($n = 6$), *Atg16l1*$^{fl/fl}$ ($n = 7$), *Atg16l1*$^{fl/fl}$*-LysM-Cre* ($n = 7$), WT C57BL/6J ($n = 6$), and *Rubicon*$^{-/-}$ ($n = 6$) mice. **(E, F)** The proportion of *M. tuberculosis* infected (*Mtb*-GFP$^+$) and the median fluorescence intensity of *Mtb*-GFP in infected alveolar macrophage (Alv. Mac.), eosinophils (Eos.), neutrophils (Neut.), inflammatory monocytes (Inf. Mono.), $CD11b^+$ DC, $CD103^+$ DC, and non-alveolar macrophages in the lung in *Atg5*$^{fl/fl}$ ($n = 7$) and *Atg5*$^{fl/fl}$*-LysM-Cre* ($n = 7$) mice at 14 dpi. **(G)** The proportion of viable ($Zombie^-$) alveolar macrophages, eosinophils, neutrophils, inflammatory monocytes, $CD11b^+$ DC, $CD103^+$ DC, and non-alveolar macrophages in the lung in *Atg5*$^{fl/fl}$ ($n = 8$) and *Atg5*$^{fl/fl}$*-CD11c-Cre* ($n = 7$) mice at 14 dpi. Statistical differences were determined by Student *t* test to compare the LysM-Cre or CD11c-Cre mice to their respective floxed control and *Rubicon*$^{-/-}$ mice to WT C57BL/6J mice (A–G).* $P < 0.05$, ** $P < 0.01$, *** $P < 0.001$, **** $P < 0.0001$. Differences that are not statistically significant are designated as ns. Pooled data from at least 2 separate experiments is graphed where each data point is from 1 biological replicate. The individual numerical values used to generate the graphed data in **Fig 2**, the statistical analyses performed to analyze these data, and the *p* values from these statistical tests are in **S2 Data**. DC, dendritic cell; dpi, days postinfection; WT, wild-type.

https://doi.org/10.1371/journal.pbio.3002159.g002

have reported roles for xenophagy in controlling *M. tuberculosis* replication in macrophages and DCs in cell culture in vitro [5,23–29]. However, in addition to there being no differences in bacterial burden in the lungs at 14 dpi **(Figs 1C and 2D)** [3], there was no significant difference in the proportion of macrophages, eosinophils, neutrophils, inflammatory monocytes, or DCs that were infected with *M. tuberculosis* **(Fig 2E)** and no difference in the *M. tuberculosis* burden in autophagy-deficient cells in the lungs of $Atg5^{fl/fl}$-*LysM-Cre* mice compared to $Atg5^{fl/fl}$ controls at 14 dpi **(Fig 2F).** Loss of xenophagy in bone marrow-derived macrophages (BMDMs) in vitro has also been associated with increased necrosis during *M. tuberculosis* infection [23]. However, we did not detect a difference in the viability of macrophages, inflammatory monocytes, eosinophils, neutrophils, or DCs in the lungs of $Atg5^{fl/fl}$ and $Atg5^{fl/fl}$-*Cd11c-Cre* mice at 14 dpi **(Figs 2G and S1B)**, although we cannot rule out effects on the balance of different cell death pathways. These data support that the role for autophagy in $CD11c^+$ lung macrophages and DCs early during *M. tuberculosis* infection in vivo is independent of xenophagy regulating *M. tuberculosis* replication. In addition, these data show that the elevated neutrophil abundance in *M. tuberculosis*-infected $Atg5^{fl/fl}$-*LysM-Cre* mice is not due to differences in the cell viability or the cell types infected with *M. tuberculosis* but instead is driven by an imbalanced inflammatory response.

Autophagy regulates proinflammatory responses in macrophages during *M. tuberculosis* infection

We have previously shown that lungs of $Atg5^{fl/fl}$-*LysM-Cre* mice at 14 dpi contain higher levels of G-CSF and IL-17A than control mice [3], cytokines that promote neutrophil development and recruitment. At this time point, the primary $CD11c^+$ cell types that are infected by *M. tuberculosis* are the lung macrophages, encompassing alveolar and interstitial macrophages [35,36]. Therefore, we hypothesized that autophagy could be suppressing the production of these cytokines from *M. tuberculosis*-infected macrophages. We tested this hypothesis by culturing BMDMs from $Atg5^{fl/fl}$, $Atg5^{fl/fl}$-*LysM-Cre*, $Atg16l1^{fl/fl}$, $Atg16l1^{fl/fl}$-*LysM-Cre*, $Becn1^{fl/fl}$, and $Becn1^{fl/fl}$-*LysM-Cre* mice and infecting with *M. tuberculosis* in vitro before monitoring cytokine and chemokine production using a cytokine bead array (Bio-Rad) on the supernatants from infected cultures **(Figs 3A–3F and S2)**. Of the 23 cytokines tested, we detected significantly higher levels of IL-1β, G-CSF, KC, TNF-α, and RANTES from the $Atg5^{fl/fl}$-*LysM-Cre* macrophage cultures compared to controls at 24 hpi **(Fig 3A–3E)**, despite no difference in bacterial burdens or BMDM viability at this time point **(Figs 3F and S2A)**, indicating that the heightened proinflammatory response of $Atg5^{-/-}$ BMDMs was not in response to increased antigen or macrophage cell death. The levels of these cytokines were only different following *M. tuberculosis* infection and not in mock-infected cultures, indicating that the increased proinflammatory responses were infection induced. The higher levels of G-CSF and KC, both proinflammatory signals associated with neutrophil inflammation [37–39], produced from *Atg5*-deficient macrophages in response to *M. tuberculosis* infection were dose dependent and confirmed by ELISA **(Fig 3H and 3I)**. Similar to $Atg5^{fl/fl}$-*LysM-Cre* BMDMs, $Atg16l1^{fl/fl}$-*LysM-Cre* BMDMs also produced higher levels of IL-1β, G-CSF, and TNF-α following *M. tuberculosis* infection in vitro **(Fig 3A, 3B and 3D)**. $Becn1^{fl/fl}$-*LysM-Cre* BMDMs also produced more IL-1β and G-CSF following *M. tuberculosis* infection in vitro compared to control cells (**Figs 3A, 3B and S2**) despite no difference in *M. tuberculosis* burden at this time point (**Fig 3F**). In addition, $Becn1^{fl/fl}$-*LysM-Cre* BMDMs produced higher levels of IL-6, MIP-1α, MIP-1β, and MCP-1 following *M. tuberculosis* infection (**Figs 3G and S2**). IL-6 in particular is associated with neutrophil recruitment [40–43] and also trended higher in *M. tuberculosis*-infected $Atg5^{fl/fl}$-*LysM-Cre* BMDMs **(Fig 3G)**, so we further analyzed the levels of IL-6

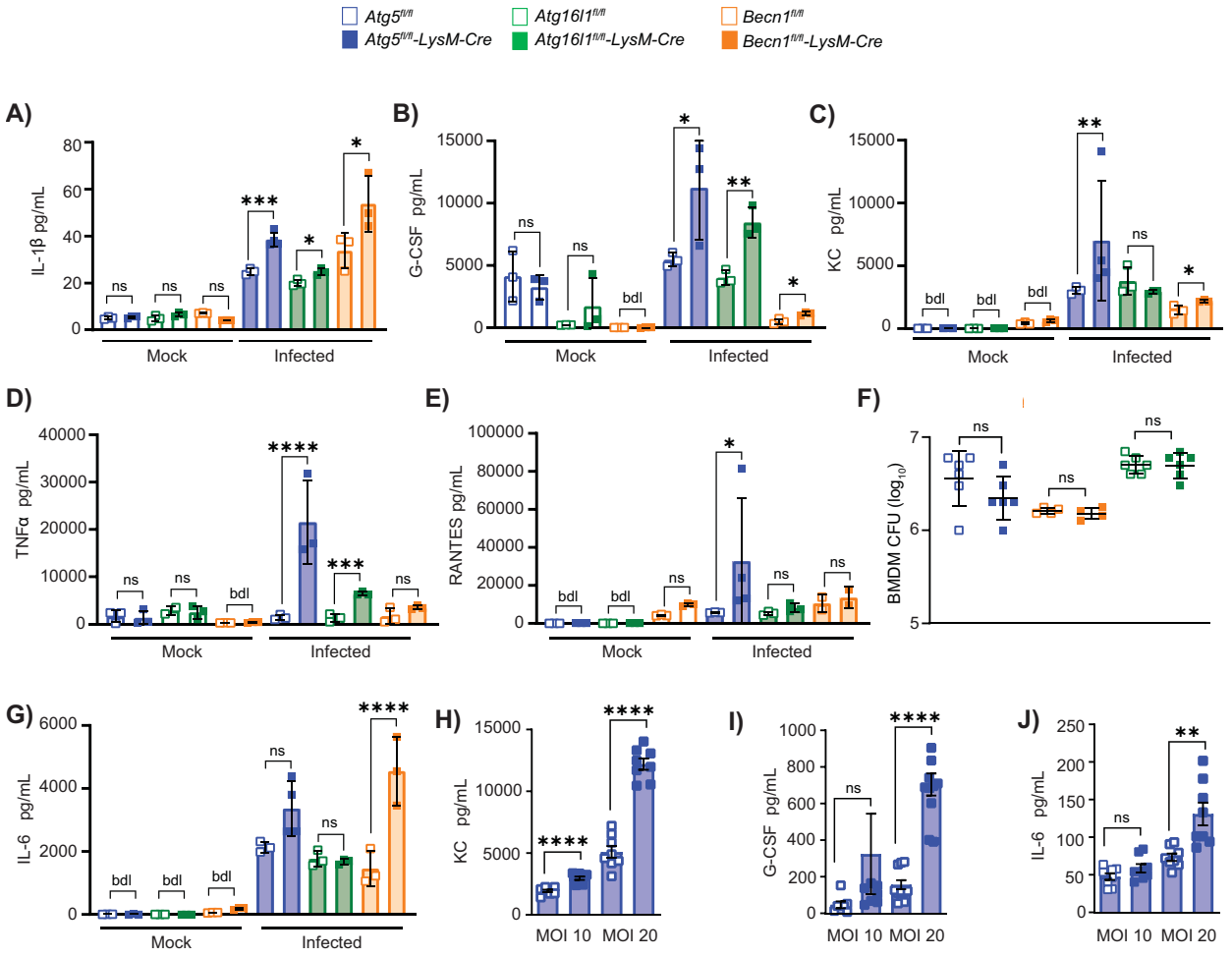

Fig 3. Autophagy regulates proinflammatory responses in macrophages during *M. tuberculosis* infection. **(A)** Cytokine bead array data to quantify cytokines in culture supernatants from *Atg5*$^{fl/fl}$, *Atg5*$^{fl/fl}$*-LysM-Cre*, *Atg16l1*$^{fl/fl}$, *Atg16l1*$^{fl/fl}$*-LysM-Cre*, *Becn1*$^{fl/fl}$, or *Becn1*$^{fl/fl}$*-LysM-Cre* BMDMs mock-treated or infected with *Mtb*-GFP at an MOI of 10 for 24 h. BMDMs generated from at least 3 mice were tested in duplicate to quantify cytokine production. **(A)** IL-1β, **(B)** G-CSF, **(C)** KC, **(D)** TNF-α, and **(E)** RANTES levels at 24 hpi are shown. **(F)** BMDM CFU counts at 24 hpi. **(G)** IL-6 levels at 24 hpi are shown. **(H)** KC, **(I)** G-CSF, and **(J)** IL-6 levels at 24 hpi in *Atg5*$^{fl/fl}$ ($n = 8$) and *Atg5*$^{fl/fl}$*-LysM-Cre* ($n = 8$) BMDMs infected with *M. tuberculosis* at an MOI of 10 or 20 for 24 h determined by ELISA. Statistical differences were determined by Student *t* test to compare the autophagy gene-deficient cells to their respective floxed control cells (A–J). * $P < 0.05$, ** $P < 0.01$, *** $P < 0.001$, **** $P < 0.0001$. Differences that are not statistically significant are designated as ns. Cytokine levels below detection limits are designated as dbl. Each data point is 1 biological replicate, and the samples were generated from at least 2 separate experiments. The individual numerical values used to generate the graphed data in **Fig 3**, the statistical analyses performed to analyze these data, and the *p* values from these statistical tests are in **S3 Data.** BMDM, bone marrow-derived macrophage; hpi, hours postinfection.

https://doi.org/10.1371/journal.pbio.3002159.g003

produced by *M. tuberculosis*-infected *Atg5*$^{fl/fl}$*-LysM-Cre* BMDMs using an ELISA (**Fig 3J**). These analyses confirmed higher levels of IL-6 secretion from *M. tuberculosis*-infected *Atg5*$^{fl/fl}$*-LysM-Cre* BMDMs compared to controls. We were able to detect more cytokines and chemokines being differentially produced by *M. tuberculosis*-infected BMDMs than what was previously detected in the lungs of *Atg5*$^{fl/fl}$*-LysM-Cre* mice at 14 dpi [3]. This is likely due to the dilution of signals produced by macrophages in the context of the total lung homogenate, decreasing our sensitivity to detect macrophage-specific responses. In addition, it is possible that the inflammatory responses of BMDMs differ from lung macrophages and DCs during *M. tuberculosis* infection. Nonetheless, loss of expression of the autophagy proteins ATG5, ATG16L1, or BECLIN 1 in macrophages both in vivo and in vitro results in higher levels of

cytokines and chemokines that are associated with neutrophil recruitment and accumulation following *M. tuberculosis* infection relative to controls, indicating that canonical autophagy is required in macrophages to control proinflammatory responses during *M. tuberculosis* infection without affecting *M. tuberculosis* burden in macrophages.

Autophagy suppresses neutrophil recruitment early during *M. tuberculosis* infection independent of mitophagy and inflammasome activation

Autophagy has been shown to suppress proinflammatory responses by negatively regulating inflammasome activation indirectly through regulation of NFκB signaling and directly by degrading pro-IL-1β and clearance of inflammasome components [44–46], which can otherwise promote proinflammatory responses, IL-1β secretion, and neutrophil recruitment [44,45,47–49]. Indeed, *Atg5*$^{fl/fl}$*-LysM-Cre*, *Atg16l1*$^{fl/fl}$*-LysM-Cre*, and *Becn1*$^{fl/fl}$*-LysM-Cre* BMDMs produce significantly more IL-1β in response to *M. tuberculosis* infection in vitro at 24 hpi compared to control BMDMs (**Fig 3A**), supporting that loss of autophagy has resulted in increased inflammasome activation. The primary inflammasome activated during *M. tuberculosis* infection of macrophages is the NLRP3 inflammasome, which consists of the NOD-, LRR-, and pyrin-domain containing protein 3 (NLRP3) sensor, ASC adaptor, and CASPASE 1 [50–53]. TLR engagement and NFκB activation during *M. tuberculosis* infection constitute the priming step of inflammasome activation, resulting in increased expression of pro-IL-1β and NLRP3 [54,55]. Phagocytosis of *M. tuberculosis* and subsequent Esx-1-dependent plasma membrane damage leading to potassium efflux is the second signal promoting NLRP3 inflammasome formation, which mediates CASPASE 1 activation followed by IL-1β processing and secretion [26,29].

To determine whether the increased neutrophil inflammation following *M. tuberculosis* infection in autophagy-deficient mice results from increased inflammasome activation, we crossed *Caspase1/11*$^{-/-}$ mice to *Atg5*$^{fl/fl}$*-LysM-Cre* and *Becn1*$^{fl/fl}$*-LysM-Cre* mice and monitored neutrophil abundance in the lungs at 14 dpi. *Caspase1/11*$^{-/-}$*/Atg5*$^{fl/fl}$*-LysM-Cre* and *Caspase1/11*$^{-/-}$*/Becn1*$^{fl/fl}$*-LysM-Cre* mice had similar neutrophil abundances and bacterial burdens in the lungs at 14 dpi as *Atg5*$^{fl/fl}$*-LysM-Cre* mice and *Becn1*$^{fl/fl}$*-LysM-Cre* mice, respectively (**Fig 4A and 4B**), indicating that increased neutrophil recruitment in the absence of autophagy is occurring independent of CASPASE1/11. *Caspase1/11* deletion also did not extend the survival of *Atg5*$^{fl/fl}$*-LysM-Cre* mice, indicating that increased inflammasome activation does not contribute to the early susceptibility of these mice (**Fig 4C**).

Autophagy has also been shown to suppress inflammatory responses via the process of mitophagy, where autophagy targets old and damaged mitochondria to the lysosome for degradation [56,57]. The build-up of damaged or dysfunctional mitochondria in the absence of autophagy results in loss of mitochondrial membrane potential and the release of reactive oxygen species (ROS), mitochondrial DNA, and ATP to the cytosol where it can lead to oxidative damage, inflammasome activation, and proinflammatory cytokine production [57–61]. Mitophagy requires the canonical autophagy proteins, including ATG5, ATG16L1, and BECLIN 1, as well as PARKIN and PTEN-induced kinase 1 (PINK1) [62]. PINK1 accumulates on damaged mitochondria and activates the mitochondrial E3 ubiquitin ligase, PARKIN, to ubiquitinylate damaged mitochondria [58,61]. Optineurin and NDP52 are the main mitophagy receptors that interact with the ubiquitinylated mitochondria and LC3, leading to autophagosome engulfment of the mitochondria [58,63]. To investigate whether loss of mitophagy could contribute to higher neutrophil accumulation in the lungs following *M. tuberculosis* infection, we measured neutrophil frequency in the lungs at 14 dpi by flow cytometry in *Parkin*$^{-/-}$ and *Pink1*$^{-/-}$ mice relative to WT controls. There was no difference in neutrophil abundance or

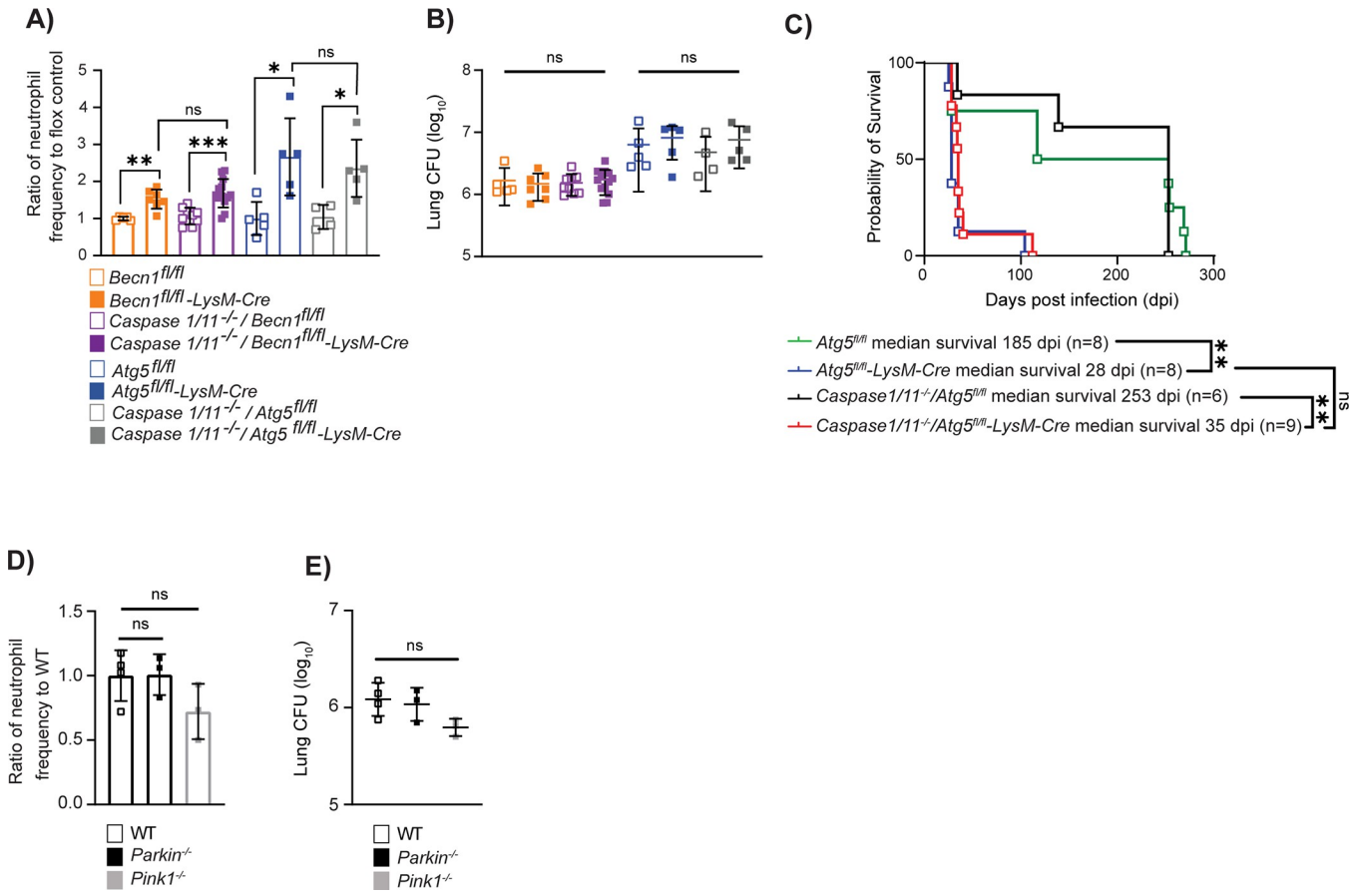

Fig 4. Autophagy suppresses neutrophil recruitment independent of mitophagy and inflammasome activation during *M. tuberculosis* infection. (A) Proportion of $CD45^+$ cells that are neutrophils ($CD45^+Ly6G^+CD11b^+$) in the lung at 14 dpi in *Mtb*-GFP infected *Becn1*$^{fl/fl}$ ($n = 5$), *Becn1*$^{fl/fl}$*-LysM-Cre* ($n = 7$), *Caspase1/11*$^{-/-}$*/Becn1*$^{fl/fl}$ ($n = 9$), *Caspase1/11*$^{-/-}$*/Becn1*$^{fl/fl}$*-LysM-Cre* ($n = 13$), *Atg5*$^{fl/fl}$ ($n = 5$), *Atg5*$^{fl/fl}$*-LysM-Cre* ($n = 5$), *Caspase1/11*$^{-/-}$*/Atg5*$^{fl/fl}$ ($n = 4$), or *Caspase1/11*$^{-/-}$*/Atg5*$^{fl/fl}$*-LysM-Cre* ($n = 5$) mice reported as a ratio relative to the average neutrophil frequency in corresponding floxed control mice. **(B)** Lung burden at 14 dpi from right lobes of the lung in *Mtb*-GFP infected *Becn1*$^{fl/fl}$ ($n = 5$), *Becn1*$^{fl/fl}$*-LysM-Cre* ($n = 7$), *Caspase1/11*$^{-/-}$*/Becn1*$^{fl/fl}$ ($n = 9$), *Caspase1/11*$^{-/-}$*/Becn1*$^{fl/fl}$*-LysM-Cre* ($n = 13$), *Atg5*$^{fl/fl}$ ($n = 5$), *Atg5*$^{fl/fl}$*-LysM-Cre* ($n = 5$), *Caspase1/11*$^{-/-}$*/Atg5*$^{fl/fl}$ ($n = 4$), or *Caspase1/11*$^{-/-}$*/Atg5*$^{fl/fl}$*-LysM-Cre* ($n = 5$) mice. The legend in 4A should be used for 4B too. **(C)** Kaplan–Meier curve of survival proportions during *Mtb*-GFP infection of *Atg5*$^{fl/fl}$, *Atg5*$^{fl/fl}$*-LysM-Cre*, *Caspase1/11*$^{-/-}$*/Atg5*$^{fl/fl}$, and *Caspase1/11*$^{-/-}$*/Atg5*$^{fl/fl}$*-LysM-Cre* mice. **(D)** Proportion of $CD45^+$ cells that are neutrophils ($CD45^+Ly6G^+CD11b^+$) in the lung at 14 dpi in *Mtb*-GFP infected WT ($n = 4$), *Parkin*$^{-/-}$ ($n = 3$), or *Pink1*$^{-/-}$ ($n = 3$) mice reported as a ratio relative to the average neutrophil frequency in WT mice. **(E)** Lung burden from the right lobe of the lung at 14 dpi in *Mtb*-GFP infected WT ($n = 4$), *Parkin*$^{-/-}$ ($n = 3$), or *Pink1*$^{-/-}$ ($n = 3$) mice. Statistical differences were determined by log-rank Mantel–Cox test (C) and one-way ANOVA and Šídák multiple comparison test (A, B, D, and E). * $P < 0.05$, ** $P < 0.01$, *** $P < 0.001$, **** $P < 0.0001$. Differences that are not statistically significant are designated as ns. Pooled data from at least 2 separate experiments is graphed where each data point is from 1 biological replicate. The individual numerical values used to generate the graphed data in Fig 4, the statistical analyses performed to analyze these data, and the *p* values from these statistical tests are in S4 Data. dpi, days postinfection; WT, wild-type.

https://doi.org/10.1371/journal.pbio.3002159.g004

bacterial burdens in *M. tuberculosis*-infected *Parkin*$^{-/-}$ or *Pink1*$^{-/-}$ mice relative to WT mice at 14 dpi (Fig 4D and 4E), indicating that mitophagy is not required to control neutrophil recruitment early during *M. tuberculosis* infection. To determine if mitophagy is required in macrophages to control proinflammatory cytokine and chemokine production during *M. tuberculosis* infection, we generated BMDMs from *Parkin*$^{-/-}$, *Pink1*$^{-/-}$, and WT mice and infected the macrophages with *M. tuberculosis* for 24 h. We measured cytokine and chemokine levels from mock and *M. tuberculosis*-infected cultures using the cytokine bead array (Bio-Rad). Unlike in autophagy-deficient BMDMs, there were no differences in IL-6, IL-1β, G-CSF, KC, TNF-α, or RANTES production by *M. tuberculosis*-infected *Parkin*$^{-/-}$ and *Pink1*$^{-/-}$ macrophages at 24 hpi compared to WT macrophages (S3 Fig), nor any differences in bacterial

burden (S3 Fig). Therefore, loss of mitophagy in macrophages does not result in higher levels of inflammation early during *M. tuberculosis* infection.

ATG5 is required to suppress early T_H17 responses in the lungs during *M. tuberculosis* infection

The higher levels of IL-17A observed in the lungs of *Atg5*$^{fl/fl}$*-LysM-Cre* mice at 14 dpi with *M. tuberculosis* relative to controls was not reproduced by BMDMs infected with *M. tuberculosis* for 24 h (S2 Fig). Although there are many reasons to explain this, one possibility is that the macrophages were not the source of IL-17A in vivo. We investigated what cell type was expressing higher levels of IL-17A in the *Atg5*$^{fl/fl}$*-LysM-Cre* mice during *M. tuberculosis* infection by crossing the *Atg5*$^{fl/fl}$ and *Atg5*$^{fl/fl}$*-LysM-Cre* mice with an IL-17A reporter mouse that expresses GFP under the IL-17A promoter (Jax # 018472). We infected *Il17a-GFP/Atg5*$^{fl/fl}$ and *Il17a-GFP/Atg5*$^{fl/fl}$*-LysM-Cre* mice with *M. tuberculosis* and monitored GFP expression as a proxy of IL-17A expression in immune cells at 14 dpi. The only cell type we reproducibly detected >0.5% of the cells expressing GFP were $CD4^+$ T cells. Similar to previous studies with *Atg5*$^{fl/fl}$ and *Atg5*$^{fl/fl}$*-LysM-Cre* mice, there was no difference in total $CD4^+$ T cell numbers in the lungs of *Il17a-GFP/Atg5*$^{fl/fl}$ and *Il17a-GFP/Atg5*$^{fl/fl}$*-LysM-Cre* mice at 14 dpi (Fig 5A) [3]. However, a greater frequency and number of the $CD4^+$ T cells in the lungs of *Il17a-GFP/Atg5*$^{fl/fl}$*-LysM-Cre* mice at 14 dpi were IL-17-GFP^+ compared to *Il17a-GFP/Atg5*$^{fl/fl}$ mice (Fig 5B and 5C). These data indicate that $CD4^+$ T cells contribute to the higher levels of IL-17A in the lungs of *M. tuberculosis*-infected *Atg5*$^{fl/fl}$*-LysM-Cre* mice and ATG5 is required in innate immune cells to negatively regulate T_H17 responses during *M. tuberculosis* infection.

IL-17A drives neutrophil influx by promoting the production of neutrophil chemokines MIP-1α and KC and through activation of endothelial cells [64–66]. Therefore, the increased T_H17 responses could be responsible for the early influx and accumulation of neutrophils in the lungs of *M. tuberculosis*-infected *Atg5*$^{fl/fl}$*-LysM-Cre* mice. To determine if the increased expression of IL-17A by T cells was responsible for the enhanced influx of neutrophils at 14 dpi in *Atg5*$^{fl/fl}$*-LysM-Cre* mice, we depleted $CD4^+$ T cells by administering antibodies specific for CD4 from day −2 to 14 dpi (Fig 5D and 5E). At 14 dpi, we harvested the lungs for enumeration of *M. tuberculosis* burden and neutrophil abundance and found that there was no effect of $CD4^+$ T cell depletion on either readout (Fig 5F and 5G). In addition, blocking IL-17A signaling by administering an anti-IL-17A antibody from day −1 to 14 dpi (Fig 5H) did not affect *M. tuberculosis* burden (Fig 5I) or neutrophil abundance (Fig 5J) in *Atg5*$^{fl/fl}$*-LysM-Cre* mice and *Atg5*$^{fl/fl}$ mice at 14 dpi. Therefore, although ATG5 is required in innate immune cells to suppress IL-17A expression in T cells, this role does not contribute to regulating neutrophil accumulation early during *M. tuberculosis* infection.

Discussion

Atg5$^{fl/fl}$*-LysM-Cre* mice are extremely susceptible to *M. tuberculosis* infection, where neutrophils accumulate in the lungs of infected *Atg5*$^{fl/fl}$*-LysM-Cre* mice by 14 dpi and are sustained at high levels until the mice succumb to the infection between 30 and 40 dpi [3]. It was previously unknown how ATG5 imparted control of neutrophil recruitment to the lungs during *M. tuberculosis* infection. We have discovered that ATG5 is required in $CD11c^+$ lung macrophages and DCs to regulate proinflammatory cytokine production and neutrophil accumulation in the lungs early during *M. tuberculosis* infection. This role for ATG5 is shared with ATG16L1 and BECLIN 1, but not RUBICON, indicating it is autophagy dependent and does not involve LAP. We were able to reproduce the heightened proinflammatory responses in *M. tuberculosis*-infected autophagy-deficient BMDMs in vitro, suggesting that autophagy specifically

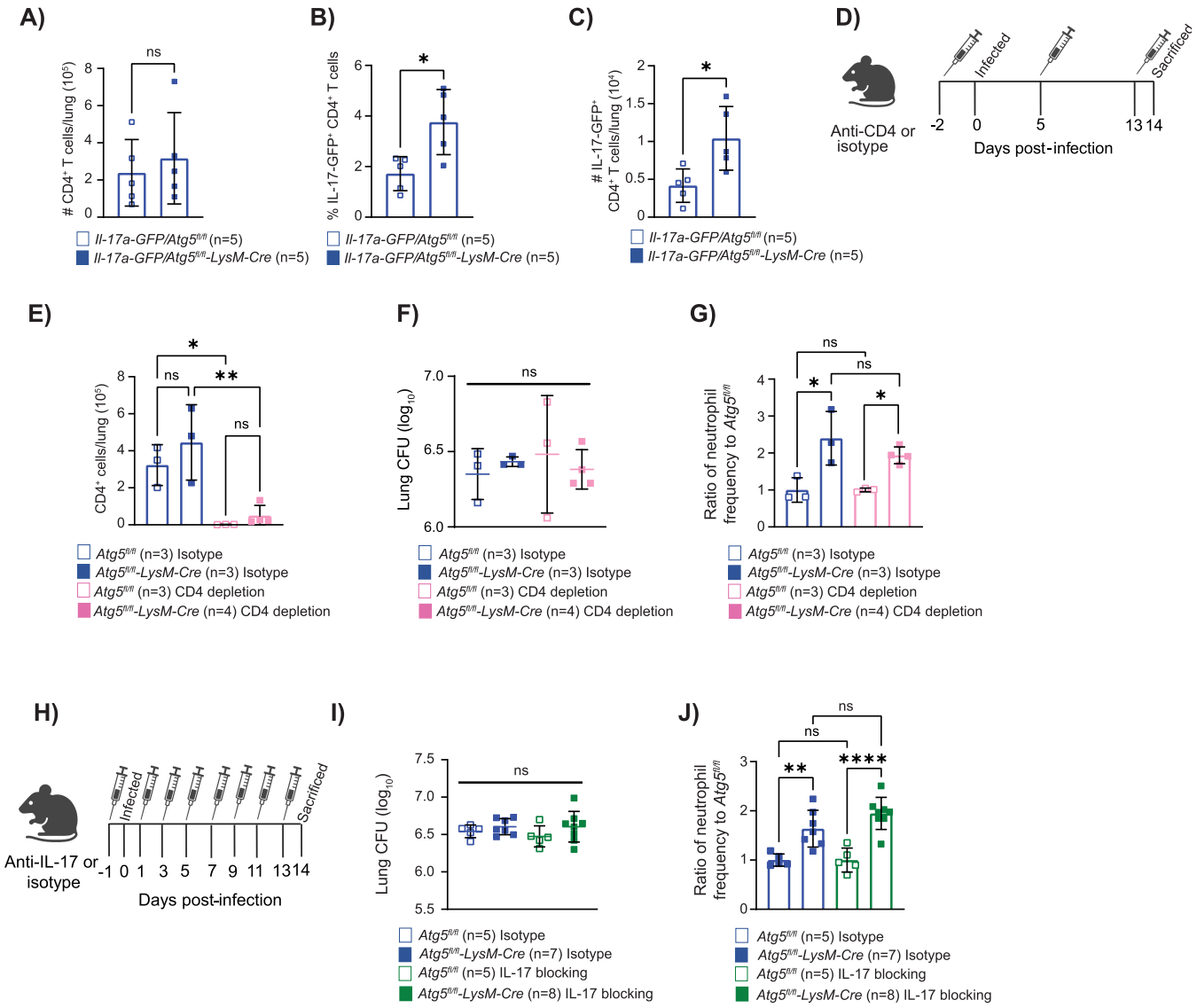

Fig 5. ATG5 is required to suppress early T_H17 responses during *M. tuberculosis* infection. (A) The number of $CD4^+$ T cells ($CD45^+$ $TCR\beta^+$ $CD4^+$) in $Atg5^{fl/fl}$ and $Atg5^{fl/fl}$-*LysM-Cre* mice are reported as the total cells per lung in the left lobe at 14 dpi. **(B)** The frequency of IL-17-GFP^+ $CD4^+$ T cells in the lung ($CD45^+$ $TCR\beta^+$ $CD4^+$ IL-17-GFP^+) of $Atg5^{fl/fl}$ and $Atg5^{fl/fl}$-*LysM-Cre* mice are reported as the percentage of $CD4^+$ T cells that are IL-17-GFP positive at 14 dpi. **(C)** The number IL-17-GFP^+ $CD4^+$ T cells in $Atg5^{fl/fl}$ and $Atg5^{fl/fl}$-*LysM-Cre* mice are reported as the total cells per lung in the left lobe at 14 dpi. **(D)** Schematic depicting the timing of CD4-depletion antibody injections. **(E)** The number of $CD4^+$ T cells ($CD45^+$ $TCR\beta^+$ $CD4^+$) in *Mtb*-GFP infected $Atg5^{fl/fl}$ and $Atg5^{fl/fl}$-*LysM-Cre* mice are reported as the total cells per lung in the left lobe at 14 dpi following antibody treatment. **(F)** Lung burden from the right lobes of the lung at 14 dpi in *Mtb*-GFP infected $Atg5^{fl/fl}$ or $Atg5^{fl/fl}$-*LysM-Cre* mice that received isotype or CD4-depletion antibodies. **(G)** Proportion of $CD45^+$ cells that are neutrophils ($CD45^+Ly6G^+CD11b^+$) in the lung at 14 dpi in *Mtb*-GFP infected $Atg5^{fl/fl}$ or $Atg5^{fl/fl}$-*LysM-Cre* mice that received CD4-depletion or isotype treatment. Neutrophil frequency is reported as a ratio relative to the average neutrophil frequency in $Atg5^{fl/fl}$ control mice at 14 dpi. **(H)** Schematic depicting delivery of the IL-17 neutralizing antibody treatments. **(I)** Lung burden from the right lobes of the lung at 14 dpi in *Mtb*-GFP infected $Atg5^{fl/fl}$ or $Atg5^{fl/fl}$-*LysM-Cre* mice that received isotype or IL-17 neutralizing antibodies. **(J)** Proportion of $CD45^+$ cells that are neutrophils ($CD45^+Ly6G^+CD11b^+$) in the lung at 14 dpi in *Mtb*-GFP infected $Atg5^{fl/fl}$ or $Atg5^{fl/fl}$-*LysM-Cre* mice that received isotype or IL-17 neutralizing antibodies. Neutrophil frequency is reported as a ratio relative to the average neutrophil frequency in $Atg5^{fl/fl}$ control mice at 14 dpi. Statistical differences were determined by Student *t* test (A) or one-way ANOVA and Šídák multiple comparison test (A–C, E–G, I, and J). * $P < 0.05$, ** $P < 0.01$, *** $P < 0.001$, **** $P < 0.0001$. Differences that are not statistically significant are designated as ns. Pooled data from at least 2 separate experiments is graphed where each data point is from 1 biological replicate. The individual numerical values used to generate the graphed data in **Fig 5**, the statistical analyses performed to analyze these data, and the *p* values from these statistical tests are in **S5 Data.** The mouse and needle images used in **Fig 5** were made with an academic account on BioRender.com where BioRender's academic license (UU25CW6WGU) terms enable the use of these graphics in journal publications. dpi, days postinfection.

https://doi.org/10.1371/journal.pbio.3002159.g005

suppresses inflammatory responses from macrophages during *M. tuberculosis* infection, although this does not rule out a similar role in DCs in vivo. Alveolar macrophages are among the first cells to encounter *M. tuberculosis* in the airways and orchestrate the initial response to infection, recruiting other innate immune cells to the lung [35,36]. We postulate that similar to the BMDMs, autophagy-deficient alveolar macrophages overproduce proinflammatory signals during *M. tuberculosis* infection, leading to increased neutrophil recruitment early during infection.

The increased levels of cytokines and chemokines produced by autophagy-deficient macrophages was dependent on *M. tuberculosis* infection, demonstrating that pathogen detection was required. However, the heightened proinflammatory responses in autophagy-deficient macrophages occurred in the absence of differences in bacterial burden, indicating that the enhanced inflammatory response is not due to increased antigen. Although multiple studies have shown effects of loss of autophagy on *M. tuberculosis* burden in macrophages and DCs in vitro in cell culture [5,23–29], there was no difference in *M. tuberculosis* burden in these cell types in vivo when we detected higher levels of proinflammatory cytokine production and neutrophil influx. Therefore, the role for autophagy in regulating proinflammatory cytokine production from $CD11c^+$ lung macrophages and DCs during *M. tuberculosis* infection is independent of xenophagy controlling *M. tuberculosis* replication. *Atg5*$^{fl/fl}$*-CD11c-Cre* mice succumb to *M. tuberculosis* infection at a similar time as *Atg16l1*$^{fl/fl}$*-LysM-Cre* and *Atg7*$^{fl/fl}$*-LysM-Cre* mice [23], suggesting that loss of the role for autophagy that we have identified in $CD11c^+$ lung macrophages and DCs is responsible for the susceptibility of *Atg16l1*$^{fl/fl}$*-LysM-Cre* and *Atg7*$^{fl/fl}$*-LysM-Cre* mice to *M. tuberculosis*. These data demonstrate that autophagy is not only required in $CD11c^+$ cells to control early inflammatory responses during *M. tuberculosis* infection, but also to promote survival through the chronic phase of infection. Although the cause of this later susceptibility of *Atg5*$^{fl/fl}$*-CD11c-Cre* to *M. tuberculosis* infection is still unknown, previous studies showed that the lungs of *M. tuberculosis*-infected *Atg16l1*$^{fl/fl}$*-LysM-Cre* and *Atg7*$^{fl/fl}$*-LysM-Cre* mice harbor higher numbers of neutrophils despite equivalent bacterial burdens compared to controls at 70 dpi [23], indicating an association between continued neutrophil accumulation and susceptibility.

We ruled out the involvement of CASPASE1/11-dependent inflammasome activity and mitophagy in the autophagy-dependent regulation of neutrophil accumulation during *M. tuberculosis* infection, leaving open the question of how autophagy regulates macrophage proinflammatory responses during infection. Our understanding of the number of cellular pathways regulated by autophagy continues to grow, and there are many possible mechanisms by which autophagy could regulate inflammatory responses in macrophages [18]. One possibility is that targeting of autophagy components to intracellular *M. tuberculosis* prevents sensing of *M. tuberculosis* by cytosolic pattern recognition receptors and subsequent proinflammatory cytokine and chemokine production, without impacting *M. tuberculosis* replication. Autophagy can also regulate levels of IL-1β [44,62,67], IL-6 [32,68,69], and TNF-α [68,69] downstream of pathogen sensing, in part by negatively regulating NFκB activation [70–72]. Autophagy can both directly promote autophagic cell death and apoptosis as well as negatively regulate RIPK3-dependent necrotic cell death, all which can impact inflammatory responses [23,73–77]. Although we did not detect overall differences in the viability of autophagy-deficient cells at the time points we observed effects on cytokine and chemokine production in vivo or in vitro, the mechanism of cell death in *Atg5*$^{fl/fl}$ and *Atg5*$^{-/-}$ cells during *M. tuberculosis* infection may vary and could impact the inflammatory responses [73,74,78]. Autophagy may also be required in macrophages for the efficient removal of dead or infected neutrophils from the lung and resolution of inflammation. The best-studied process for removal of dead cells by phagocytes is efferocytosis [79]. LAP has specifically been shown to

contribute to efferocytosis [80], and although we rule out a role for LAP in regulating neutrophil accumulation during *M. tuberculosis* infection, in remains possible that processing of dead cells may be attenuated in the absence of autophagy. Another possible mechanism for how autophagy regulates inflammatory responses from macrophages during *M. tuberculosis* infection involves the process of ER-phagy. ER-phagy is induced under conditions of ER stress, accumulation of unfolded proteins, and during infection [81,82]. ER-phagy restrains ER stress responses by targeting excess or damaged endoplasmic reticulum to autophagosomes for degradation [81], but in the absence of autophagy, ER stress activates NFκB-dependent transcription of inflammatory cytokines, such as IL-1β, IL-6, IL-18, and TNF-α [82].

We also discovered that ATG5 was required in innate immune cells to suppress early T_H17 responses during *M. tuberculosis* infection. At this point, we do not know if the increased abundance of IL-17^+ $CD4^+$ T cells in *M. tuberculosis*-infected *Atg5$^{fl/fl}$-LysM-Cre* mice is due to an autophagy-dependent or independent role for ATG5, but there are multiple other reports of autophagy regulating T_H17 responses. The effect of loss of *Atg5* in innate immune cells on IL-17A expression from T cells may be explained by the requirement for autophagy in DCs to negatively regulate surface expression of disintegrin and metalloproteinase domain-containing protein 10 (ADAM10). ADAM10 cleaves its substrate ICOSL and lower levels of ICOSL leads to decreased ICOSL-ICOS interactions between DCs and T cells, resulting in less $CD25^{hi}$ $CD4^+$ T regulatory cells and more IL-17^+ $CD4^+$ T cells [83]. In addition, autophagy negatively regulates T_H17 differentiation by reducing IL-23 and IL-1β levels, which promote T_H17 differentiation and IL-17A secretion [4,84–86]. Nonetheless, depleting $CD4^+$ T cells or blocking IL-17A did not rescue the increased neutrophil accumulation in the lungs of *M. tuberculosis*-infected *Atg5$^{fl/fl}$-LysM-Cre* mice at 14 dpi, suggesting that the hyper-inflammatory responses from infected autophagy-deficient macrophages and DCs is sufficient to recruit excessive neutrophils early during infection. However, it is possible that the heightened T_H17 responses in *M. tuberculosis*-infected *Atg5$^{fl/fl}$-LysM-Cre* mice have a longer-term impact on the increased susceptibility of these mice and could contribute to the susceptibility of *Atg5$^{fl/fl}$-Cd11c-Cre* mice during the chronic phase of infection.

Our data support a role for autophagy in restricting neutrophil accumulation in the lung but does not rule out additional contributions from autophagy-independent roles for ATG5, BECLIN 1, and ATG16L1. In particular, loss of *Atg5*, *Becn1*, or *Atg16l1* in $LysM^+$ cells led to different degrees of elevated neutrophil frequency in the lung at 14 dpi relative to control mice, where loss of *Atg5* results in the greatest increase in neutrophil abundance. This could in part be due to differences in efficiency of gene deletion in the different lines [23]. In addition, we have previously identified an autophagy-independent role for ATG5 in neutrophils, where loss of ATG5 in neutrophils can result in early lethality during *M. tuberculosis* infection [3]. Therefore, loss of *Atg5* in $LysM^+$ cells, which includes neutrophils, may result in higher neutrophil frequency in the lung at 14 dpi than loss of *Becn1* or *Atg16l1* because of this autophagy-independent role for ATG5 in neutrophils. We hypothesize that the combination of the newly discovered role for autophagy in $CD11c^+$ lung macrophages and DCs to regulate inflammatory responses and an autophagy-independent role for ATG5 in neutrophils collectively allow for control of *M. tuberculosis* infection, where loss of both functions results in the extreme susceptibility of *Atg5$^{fl/fl}$-LysM-Cre* mice to *M. tuberculosis* infection. Higher abundances of neutrophils have been associated with poor disease prognosis and treatment outcomes in TB patients [14–16]. Therefore, our new findings and future dissection of the ATG5-dependent mechanisms of regulating neutrophil recruitment to the lungs during *M. tuberculosis* infection will provide critical insight into how to promote protective immune responses to TB.

Materials and methods

Mice

All flox mice (*Atg5*$^{fl/lfl}$, *Atg16l1*$^{fl/fl}$, and *Becn1*$^{fl/fl}$) used in this study have been described previously [3,87–89] and colonies are maintained in an enhanced barrier facility. LysM-Cre (Jax #004781), Cd11c-Cre (Jax #007567), Mrp8-Cre (Jax #021614) from the Jackson Laboratory were crossed to specific flox mice. *Il17a-IRES-GFP-KI* (Jax # 018472) reporter mice were bred to *Atg5*$^{fl/fl}$*-LysM-Cre* and *Atg5*$^{fl/fl}$ mice to generate the *Il17a-GFP/Atg5*$^{fl/fl}$*-LysM-Cre* and *Il17a-GFP/Atg5*$^{fl/fl}$ lines. *Rubicon*$^{-/-}$ (Jax # 032581) and WT littermates were provided by D. Green and J. Martinez [90]. Caspase 1/11$^{-/-}$ (Jax #016621) were bred to *Atg5*$^{fl/fl}$*-LysM-Cre* and *Becn1*$^{fl/fl}$*-LysM-Cre* mice. *Parkin*$^{-/-}$ (Jax # 006582) [91], *Pink1*$^{-/-}$ (Jax # 017946) [56], and WT control mice were a gift from Dr. Jonathan Brestoff at Washington University School of Medicine. Male and female littermates (aged 6 to 12 weeks) were used and were subject to randomization. A minimum of 3 mice were used per experiment and each experiment was performed twice. Statistical consideration was not used to determine mouse sample sizes. The mice were housed and bred at Washington University in St. Louis in specific pathogen-free conditions in accordance with federal and university guidelines, and protocols were approved by the Animal Studies Committee of Washington University.

Infection of mice with *M. tuberculosis* and measurement of bacterial burden in the lungs

M. tuberculosis Erdman expressing GFP (*Mtb*-GFP [10,92]) was used in all experiments except experiments with the *Il-17a-GFP/Atg5*$^{fl/fl}$*-LysM-Cre* reporter mice when WT Erdman was used. *M. tuberculosis* was cultured at 37˚C in 7H9 (broth) or 7H11 (agar) (Difco) medium supplemented with 10% oleic acid/albumin/dextrose/catalase (OADC), 0.5% glycerol, and 0.05% Tween 80 (broth). Cultures of GFP expressing *M. tuberculosis* were grown in the presence of kanamycin (20 μg/mL) to ensure plasmid retention. *M. tuberculosis* cultures in logarithmic growth phase (OD600 = 0.5–0.8) were washed with PBS + 0.05% Tween-80, sonicated to disperse clumps, and diluted in sterile water before delivering 100 CFUs of aerosolized *M. tuberculosis* per lung using an Inhalation Exposure System (Glas-Col). Within 2 h of each infection, lungs were harvested from at least 2 control mice, homogenized, and plated on 7H11 agar to determine the input CFU dose. At 14 dpi, *M. tuberculosis* titers were determined by homogenizing the superior, middle, and inferior lobes of the right lung and plating serial dilutions on 7H11 agar. Colonies were counted after 3 weeks of incubation at 37˚C in 5% CO_2.

Flow cytometry from blood and infected lungs

Blood was collected by cardiac puncture into K2EDTA anticoagulant tubes (BD, 365974). Red blood cell lysis was performed by adding 2 mL of ACK lysis buffer (Gibco, A10492-01) per 100 μL of EDTA-treated blood for 5 min at room temperature. Cells were pelleted at 500×g for 5 min and then resuspended in 50 μL of PBS + 2% HI-FBS + 2 mM EDTA in the presence of Fc receptor blocking antibody (BioLegend, 101302). Cells were labeled with antibodies as described below. Lungs were perfused with sterile PBS and digested for 1 h with 625 μg/mL collagenase D (Roche 11088875103) and 75 U/mL DNase I (Sigma D4527). Cells were quenched with PBS + 2% heat-inactivated (HI)-FBS, + 2 mM EDTA and passed through a 70 μm filter. Cells were stained with Zombie-violet or Zombie-NIR in PBS at 1:2,000 dilution for 5 min at room temperature prior to resuspending in PBS + 2% HI-FBS + 2 mM EDTA in the presence of Fc receptor blocking antibody (BioLegend, 101302) for blocking. Cells were labeled with antibodies at a 1:200 dilution using the following mouse markers: CD11b_BV605

or PerCP-Cy5.5 (clone M1/70), CD45_AF700 (BioLegend, 103259), Ly6G_PE-Cy7 or AF647 (clone 1A8), MHCII_Spark blue 550 (BioLegend, 107662), CD62L_Pe/Cy5 (BioLegend, 104410), CD44_BV510 (BioLegend, 103044), CD11c_PerCP (BioLegend, 117325), Ly6C_BV605 (BioLegend, 128036), CD4_BV570 (clone RM4-5), TCRb_BV421 (clone H57-597), CD19_Pacific blue (BioLegend, 115526), Zombie-violet or -NIR (BioLegend, 423113 or 423105), SiglecF_BV480 (BD Biosciences, 746668), MHC-II_Sparkblue550 (BioLegend, 107662), CD64_PerCP-eFluor 710 (eBiosciences, 46061482) and MerTK_PE/Cy7 (eBiosciences, 25575182). Cells were incubated for 20 min at 4˚C with antibodies, washed and then fixed in 4% paraformaldehyde (Electron Microscope Sciences) for 20 min at room temperature. Flow cytometry was performed on an LSR-Fortessa (BD Bioscience) or an Aurora (Cytek Biosciences, with 4 laser 16V-14B-10YG-8R configuration) and analyzed using FlowJo software (Tree Star). Absolute cell counts were determined using Precision count beads (BioLegend) or volumetric-based counting on the Aurora. Gating strategies to identify *Mtb*-GFP$^+$ myeloid cell populations, viable lung neutrophils, CD4$^+$ T cells and IL-17-GFP$^+$ CD4$^+$ T cells are in S4A–S4C Fig.

Culturing and infection of bone marrow-derived macrophages (BMDMs)

BMDMs were generated by flushing femurs and tibias of mice and culturing the cells in DMEM, 20% HI-FBS, 10% supernatant from 3T3 cells overexpressing M-CSF + 1% MEM non-essential amino acids (Cellgro 25-025-CI), 2 mM L-glutamine, 100 U/mL penicillin, and 100 μg/mL streptomycin (Sigma P4333) at 37˚C in 5% CO_2 in non-TC treated plates. After 6 days, non-adherent cells were removed and 1×10^6 adherent macrophages were seeded per well in 6-well non-TC treated plates in DMEM, 10% HI-FBS, 1% MEM non-essential amino acids, and 2 mM L-glutamine. BMDMs were rested overnight at 37˚C in 5% CO_2. *M*. *tuberculosis* was grown to an OD of 0.6 to 0.8, washed with PBS twice, sonicated to disperse clumps, centrifuged at 55×g for 10 min to remove clumps and resuspended in antibiotic-free BMDM media. Macrophages were infected at an MOI of 10 by centrifuging the cells at 200×g for 10 min. BMDMs were washed with PBS twice to remove free *M*. *tuberculosis* and fresh BMDM media was added to each well. Cells were incubated at 37˚C and 5% CO_2 for 24 h. To determine CFU counts, the cells were lysed with 0.05% triton X-100, serially diluted, and plated onto 7H11 agar and incubated for 21 days when bacterial colonies were counted. At 24 hours postinfection (hpi), supernatants were stored at −80˚C for cytokine analysis. To assess BMDM viability, cells were harvested at 24 hpi by gently scrapping, washed with PBS twice, stained with Zombie-violet in PBS at 1:2,000 dilution for 5 min at room temperature, washed once with PBS, and fixed in 4% PFA for 20 min at room temperature before performing flow cytometry. Flow cytometry was performed on an LSR-Fortessa (BD Bioscience) and analyzed using FlowJo software (Tree Star). The gating strategy to identify viable BMDMs at 24 hpi is depicted in S1D Fig.

Cytokine analysis

BMDM supernatants were filtered through a 0.22 μm filter twice to remove *M*. *tuberculosis* and analyzed using the BioPlex-Pro Mouse Cytokine 23-Plex Immunoassay (Bio-Rad) as per the manufacturer's instructions. ELISAs were performed according to the manufacturer's instructions (R&D systems): KC/CXCL1 (DY453), IL-6 (DY406), and G-CSF (DY414).

IL-17A blocking and T cell depletion

To neutralize IL-17A, 100 μg of InVivo monoclonal anti-IL-17A (Bio X Cell, BE0173) neutralizing antibody was administered to *Atg5*$^{fl/fl}$ and *Atg5*$^{fl/fl}$*-LysM-Cre* mice by intraperitoneal (i.p.)

injection every other day starting at 1 day prior to infection, with the final dose delivered at 13 dpi, similar to published protocols [93]. Control mice received 100 μg of IgG from mouse serum (Sigma, I5381) by i.p. injection every other day starting 1 day prior to infection and finishing on 13 dpi. To deplete $CD4^+$ T cells from mice, 250 μg of anti-mouse CD4 (Leinco Technologies, C1333) was administered by i.p. injection at 2 days prior to infection, 5 dpi, and 12 dpi. Control mice received 250 μg of IgG from rat serum (Sigma, 18015) i.p. on 2 days prior to infection, 5 dpi, and 12 dpi.

Data and statistics

All experiments were performed at least twice. When shown, multiple samples represent biological (not technical) replicates of mice randomly sorted into each experimental group. No blinding was performed during animal experiments. Animals were only excluded when pathology unrelated to *M. tuberculosis* infection was present (i.e., bad teeth leading to weight loss). Determination of statistical differences was performed with Prism (GraphPad Software) using log-rank Mantel–Cox test (survival), unpaired two-tailed *t* test (to compare 2 groups with similar variances), or one-way ANOVA with Šídák multiple comparison test (to compare more than 2 groups). When used, center values and error bars represent the mean +/- SEM. In all figures, all significant differences are indicated by asterisks: * $P < 0.05$, ** $P < 0.01$, *** $P < 0.001$, **** $P < 0.0001$. Nonsignificant comparisons of particular interest are noted as ns.

Supporting information

S1 Fig. ATG5 is not required in $CD11c^+$ cells to regulate neutrophil viability in the lung or accumulation of neutrophils in the blood during *M. tuberculosis* infection. (A) The proportion of lung neutrophils ($CD45^+$ $Ly6G^+$ $CD11b^+$) that are viable ($Zombie^-$) in *M. tuberculosis*-infected $Atg5^{fl/fl}$ ($n = 8$) and $Atg5^{fl/fl}$-*CD11c-Cre* ($n = 7$) mice at 14 dpi. **(B)** The proportion of $CD45^+$ cells in the blood that are neutrophils in $Atg5^{fl/fl}$ ($n = 4$ in naïve and $n = 3$ in 14 dpi) and $Atg5^{fl/fl}$-*CD11c-Cre* ($n = 4$) mice at 14 dpi and uninfected (naïve) mice. Statistical differences were determined by Student *t* test comparing the genotypes within a particular cell type or treatment group. * $P < 0.05$, ** $P < 0.01$, *** $P < 0.001$, **** $P < 0.0001$. Differences that are not statistically significant are designated as ns. Pooled data from at least 2 separate experiments are graphed where each data point is from 1 biological replicate. The individual numerical values used to generate the graphed data in S1 Fig, the statistical analyses performed to analyze these data, and the *p* values from these statistical tests are in S6 Data.
(TIF)

S2 Fig. Levels of viability, cytokines, and chemokines in autophagy-deficient macrophages during *M. tuberculosis* infection. (A) The proportion of $Atg5^{fl/fl}$ ($n = 5$) and $Atg5^{fl/fl}$-*LysM-Cre* ($n = 5$) BMDMs that are viable ($Zombie^-$) at 24 hpi in mock and *Mtb*-GFP treated groups. Cytokine bead array data from mock treated and *Mtb*-GFP infected BMDMs. $Atg5^{fl/fl}$, $Atg5^{fl/fl}$-*LysM-Cre*, $Atg16l1^{fl/fl}$, $Atg16l1^{fl/fl}$-*LysM-Cre*, $Becn1^{fl/fl}$, and $Becn1^{fl/fl}$-*LysM-Cre* BMDMs were cultured for 24 hpi, and cytokine levels were measured in the spent media from mock treated or infected macrophages. BMDMs from at least 3 mice were tested in duplicate to quantify the cytokines in the bead array. All cytokine and chemokine data that are not significantly different between $Atg5^{fl/fl}$-*LysM-Cre* and $Atg5^{fl/fl}$ mice are reported here. **(B)** IL-1α, **(C)** IL-4, **(D)** IL-10, **(E)** IL-12(p40), **(F)** IL-12(p70), **(G)** IFN-γ, **(H)** MIP1β, G **(I)** M-CSF, **(J)** MIP1α, **(K)** MCP-1, **(L)** Eotaxin, and **(M)** IL-17 levels at 24 hpi. Statistical differences were determined by one-way ANOVA and Šídák multiple comparison test (A) and Student *t* test comparing the autophagy-deficient macrophage with its floxed control within a treatment condition (B–M). *

$P < 0.05$, ** $P < 0.01$, *** $P < 0.001$, **** $P < 0.0001$. Cytokine levels below detection limits are designated as dbl. Differences that are not statistically significant are designated as ns. Each data point is 1 biological replicate, and the samples were generated from at least 2 separate experiments. The individual numerical values used to generate the graphed data in S2 Fig, the statistical analyses performed to analyze these data, and the *p* values from these statistical tests are in S7 Data.
(TIF)

S3 Fig. Mitophagy is not required in macrophages to regulate proinflammatory responses during *M. tuberculosis* infection. WT, *Parkin*$^{-/-}$ and *Pink1*$^{-/-}$, BMDMs were cultured for 24 hpi and cytokine levels were measured by cytokine bead array in the media from mock treated or *Mtb*-GFP infected macrophages. **(A)** IL-1β, **(B)** G-CSF, **(C)** IL-6, **(D)** KC, **(E)** RANTES, and **(F)** TNF-α levels at 24 hpi **(G)** BMDM CFU counts from 24 hpi. BMDMs from at least 3 mice were tested in duplicate to quantify cytokines in the bead array. Each point is 1 biological replicate. Statistical differences were determined by one-way ANOVA and Šídák multiple comparison test (A–G). * $P < 0.05$, ** $P < 0.01$, *** $P < 0.001$, **** $P < 0.0001$. Cytokine levels below detection limits are designated as dbl. Statistical differences that are not significant are designated as ns. Each data point is 1 biological replicate, and the samples were generated from at least 2 separate experiments. The individual numerical values used to generate the graphed data in S3 Fig, the statistical analyses performed to analyze these data, and the *p* values from these statistical tests are in S8 Data.
(TIF)

S4 Fig. Gating strategies for flow cytometry identification of myeloid cells and IL-17 expressing T cells in the lung or viable BMDMs. Representative flow cytometry plots depicting the gating strategy used to identify *Mtb*-GFP^{+} myeloid cells **(A)**, viable lung neutrophils **(B)**, and IL-17-GFP^{+} CD4^{+} T cells **(C)** in the lung at 14 dpi. **(D)** Representative flow cytometry plots showing the gating strategy to identify viable BMDMs at 24 hpi. FSC-A, forward scatter area; SSC-A, side scatter area; FSC-H, forward scatter height; FSC-W, forward scatter width, Alv. Mac., alveolar macrophages; Eos., eosinophils; DC, dendritic cell, and Inf. Mono., inflammatory monocytes.
(TIF)

S1 Data. Supporting data files for Fig 1. These supporting data files include the individual numerical values used to generate the graphed data in Fig 1, the statistical analyses performed to analyze these data, and the *p* value from these statistical tests.
(XLSX)

S2 Data. Supporting data files for Fig 2. These supporting data files include the individual numerical values used to generate the graphed data in Fig 2, the statistical analyses performed to analyze these data, and the *p* value from these statistical tests.
(XLSX)

S3 Data. Supporting data files for Fig 3. These supporting data files include the individual numerical values used to generate the graphed data in Fig 3, the statistical analyses performed to analyze these data, and the *p* value from these statistical tests.
(XLSX)

S4 Data. Supporting data files for Fig 4. These supporting data files include the individual numerical values used to generate the graphed data in Fig 4, the statistical analyses performed to analyze these data, and the *p* value from these statistical tests.
(XLSX)

S5 Data. Supporting data files for Fig 5. These supporting data files include the individual numerical values used to generate the graphed data in Fig 5, the statistical analyses performed to analyze these data, and the *p* value from these statistical tests.
(XLSX)

S6 Data. Supporting data files for S1 Fig. These supporting data files include the individual numerical values used to generate the graphed data in S1 Fig, the statistical analyses performed to analyze these data, and the *p* value from these statistical tests.
(XLSX)

S7 Data. Supporting data files for S2 Fig. These supporting data files include the individual numerical values used to generate the graphed data in S2 Fig, the statistical analyses performed to analyze these data, and the *p* value from these statistical tests.
(XLSX)

S8 Data. Supporting data files for S3 Fig. These supporting data files include the individual numerical values used to generate the graphed data in S3 Fig, the statistical analyses performed to analyze these data, and the *p* value from these statistical tests.
(XLSX)

Acknowledgments

The authors thank Dr. Jonathan Brestoff at Washington University School of Medicine for generously providing the *Parkin*$^{-/-}$ and *Pink1*$^{-/-}$ mice.

Author Contributions

Conceptualization: Rachel L. Kinsella, Christina L. Stallings.

Data curation: Rachel L. Kinsella, Jacqueline M. Kimmey, Asya Smirnov, Reilly Woodson, Margaret R. Gaggioli, Sthefany M. Chavez.

Formal analysis: Rachel L. Kinsella, Jacqueline M. Kimmey.

Funding acquisition: Christina L. Stallings.

Investigation: Rachel L. Kinsella.

Methodology: Rachel L. Kinsella.

Resources: Darren Kreamalmeyer.

Supervision: Christina L. Stallings.

Writing – original draft: Rachel L. Kinsella, Christina L. Stallings.

Writing – review & editing: Rachel L. Kinsella, Jacqueline M. Kimmey, Asya Smirnov, Reilly Woodson, Margaret R. Gaggioli, Sthefany M. Chavez, Darren Kreamalmeyer, Christina L. Stallings.

References

1. World Health Organization. Regional Office for South-East Asia. WHO global Tuberculosis report 2021 [Internet]. New Delhi: World Health Organization. Regional Office for South-East Asia; 2022 [cited 2022 Sep 9]. Available from: https://apps.who.int/iris/handle/10665/361162.

2. Kinsella R, Zhu D, Harrison G, Mayer Bridwell A, Prusa J, Chavez S, et al. Perspectives and Advances in the Understanding of Tuberculosis. Annu Rev Pathol. 2021 Jan 24; 16:377–408. https://doi.org/10.1146/annurev-pathol-042120-032916 PMID: 33497258
3. Kimmey JM, Huynh JP, Weiss LA, Park S, Kambal A, Debnath J, et al. Unique role for ATG5 in neutrophil-mediated immunopathology during M. tuberculosis infection. Nature. 2015 Dec; 528(7583):565–9. https://doi.org/10.1038/nature16451 PMID: 26649827
4. Castillo EF, Dekonenko A, Arko-Mensah J, Mandell MA, Dupont N, Jiang S, et al. Autophagy protects against active tuberculosis by suppressing bacterial burden and inflammation. Proc Natl Acad Sci U S A. 2012 Nov 13; 109(46):E3168–76. https://doi.org/10.1073/pnas.1210500109 PMID: 23093667
5. Watson RO, Manzanillo PS, Cox JS. Extracellular M. tuberculosis DNA Targets Bacteria for Autophagy by Activating the Host DNA-Sensing Pathway. Cell. 2012 Aug; 150(4):803–15. https://doi.org/10.1016/j.cell.2012.06.040 PMID: 22901810
6. Mishra BB, Lovewell RR, Olive AJ, Zhang G, Wang W, Eugenin E, et al. Nitric oxide prevents a pathogen-permissive granulocytic inflammation during tuberculosis. Nat Microbiol. 2017 Jul; 2(7):17072. https://doi.org/10.1038/nmicrobiol.2017.72 PMID: 28504669
7. Mishra BB, Rathinam VAK, Martens GW, Martinot AJ, Kornfeld H, Fitzgerald KA, et al. Nitric oxide controls the immunopathology of tuberculosis by inhibiting NLRP3 inflammasome–dependent processing of IL-1β. Nat Immunol. 2013 Jan; 14(1):52–60.
8. Nandi B, Behar SM. Regulation of neutrophils by interferon-γ limits lung inflammation during tuberculosis infection. J Exp Med. 2011 Oct 24; 208(11):2251–62.
9. Niazi MKK, Dhulekar N, Schmidt D, Major S, Cooper R, Abeijon C, et al. Lung necrosis and neutrophils reflect common pathways of susceptibility to *Mycobacterium tuberculosis* in genetically diverse, immune competent mice. Dis Model Mech. 2015 Jan 1;dmm.020867.
10. Nair S, Huynh JP, Lampropoulou V, Loginicheva E, Esaulova E, Gounder AP, et al. Irg1 expression in myeloid cells prevents immunopathology during M. tuberculosis infection. J Exp Med. 2018 Apr 2; 215(4):1035–45. https://doi.org/10.1084/jem.20180118 PMID: 29511063
11. Dorhoi A, Yeremeev V, Nouailles G, Weiner J, Jörg S, Heinemann E, et al. Type I IFN signaling triggers immunopathology in tuberculosis-susceptible mice by modulating lung phagocyte dynamics. Eur J Immunol. 2014 Aug; 44(8):2380–93. https://doi.org/10.1002/eji.201344219 PMID: 24782112
12. Moreira-Teixeira L, Stimpson PJ, Stavropoulos E, Hadebe S, Chakravarty P, Ioannou M, et al. Type I IFN exacerbates disease in tuberculosis-susceptible mice by inducing neutrophil-mediated lung inflammation and NETosis. Nat Commun. 2020 Dec; 11(1):5566. https://doi.org/10.1038/s41467-020-19412-6 PMID: 33149141
13. Moreira-Teixeira L, Tabone O, Graham CM, Singhania A, Stavropoulos E, Redford PS, et al. Mouse transcriptome reveals potential signatures of protection and pathogenesis in human tuberculosis. Nat Immunol. 2020 Apr; 21(4):464–76. https://doi.org/10.1038/s41590-020-0610-z PMID: 32205882
14. Carvalho ACC, Amorim G, Melo MGM, Silveira AKA, Vargas PHL, Moreira ASR, et al. Pre-Treatment Neutrophil Count as a Predictor of Antituberculosis Therapy Outcomes: A Multicenter Prospective Cohort Study. Front Immunol. 2021 Jul 2; 12:661934. https://doi.org/10.3389/fimmu.2021.661934 PMID: 34276654
15. Han Y, Kim SJ, Lee SH, Sim YS, Ryu YJ, Chang JH, et al. High blood neutrophil-lymphocyte ratio associated with poor outcomes in miliary tuberculosis. J Thorac Dis. 2018 Jan; 10(1):339–46. https://doi.org/10.21037/jtd.2017.12.65 PMID: 29600065
16. Lowe DM, Bandara AK, Packe GE, Barker RD, Wilkinson RJ, Griffiths CJ, et al. Neutrophilia independently predicts death in tuberculosis: Table 1–. Eur Respir J. 2013 Dec; 42(6):1752–7.
17. Berry MPR, Graham CM, McNab FW, Xu Z, Bloch SAA, Oni T, et al. An interferon-inducible neutrophil-driven blood transcriptional signature in human tuberculosis. Nature. 2010 Aug; 466(7309):973–7. https://doi.org/10.1038/nature09247 PMID: 20725040
18. Kinsella RL, Nehls EM, Stallings CL. Roles for Autophagy Proteins in Immunity and Host Defense. Vet Pathol. 2018 May; 55(3):366–73. https://doi.org/10.1177/0300985818754967 PMID: 29433400
19. Kimmey JM, Stallings CL. Bacterial Pathogens versus Autophagy: Implications for Therapeutic Interventions. Trends Mol Med. 2016 Dec; 22(12):1060–76. https://doi.org/10.1016/j.molmed.2016.10.008 PMID: 27866924
20. Lamb CA, Yoshimori T, Tooze SA. The autophagosome: origins unknown, biogenesis complex. Nat Rev Mol Cell Biol. 2013 Dec; 14(12):759–74. https://doi.org/10.1038/nrm3696 PMID: 24201109
21. Mizushima N, Yoshimori T, Ohsumi Y. The Role of Atg Proteins in Autophagosome Formation. Annu Rev Cell Dev Biol. 2011 Nov 10; 27(1):107–32. https://doi.org/10.1146/annurev-cellbio-092910-154005 PMID: 21801009

22. Mizushima N, Noda T, Yoshimori T, Tanaka Y, Ishii T, George MD, et al. A protein conjugation system essential for autophagy. Nature. 1998 Sep; 395(6700):395–8. https://doi.org/10.1038/26506 PMID: 9759731

23. Golovkine GR, Roberts AW, Morrison HM, Rivera-Lugo R, McCall RM, Nilsson H, et al. Autophagy restricts Mycobacterium tuberculosis during acute infection in mice. Nat Microbiol [Internet]. 2023 Apr 10 [cited 2023 Apr 11]. Available from: https://www.nature.com/articles/s41564-023-01354-6. https://doi.org/10.1038/s41564-023-01354-6 PMID: 37037941

24. Manzanillo PS, Ayres JS, Watson RO, Collins AC, Souza G, Rae CS, et al. The ubiquitin ligase parkin mediates resistance to intracellular pathogens. Nature. 2013 Sep; 501(7468):512–6. https://doi.org/10.1038/nature12566 PMID: 24005326

25. Köster S, Upadhyay S, Chandra P, Papavinasasundaram K, Yang G, Hassan A, et al. *Mycobacterium tuberculosis* is protected from NADPH oxidase and LC3-associated phagocytosis by the LCP protein CpsA. Proc Natl Acad Sci U S A [Internet]. 2017 Oct 10 [cited 2023 Apr 4]; 114(41). Available from: https://pnas.org/doi/full/ https://doi.org/10.1073/pnas.1707792114 PMID: 28973896

26. Aylan B, Bernard EM, Pellegrino E, Botella L, Fearns A, Athanasiadi N, et al. ATG7 and ATG14 restrict cytosolic and phagosomal Mycobacterium tuberculosis replication in human macrophages. Nat Microbiol [Internet]. 2023 Mar 23 [cited 2023 Apr 4]. Available from: https://www.nature.com/articles/s41564-023-01335-9. https://doi.org/10.1038/s41564-023-01335-9 PMID: 36959508

27. Dutta RK, Kathania M, Raje M, Majumdar S. IL-6 inhibits IFN-γ induced autophagy in Mycobacterium tuberculosis H37Rv infected macrophages. Int J Biochem Cell Biol. 2012 Jun; 44(6):942–54.

28. Deretic V. Autophagy in Tuberculosis. Cold Spring Harb Perspect Med. 2014 Nov 1; 4(11):a018481–a018481. https://doi.org/10.1101/cshperspect.a018481 PMID: 25167980

29. Sakowski ET, Koster S, Portal Celhay C, Park HS, Shrestha E, Hetzenecker SE, et al. Ubiquilin 1 Promotes IFN-γ-Induced Xenophagy of Mycobacterium tuberculosis. Lewinsohn DM, editor. PLoS Pathog. 2015 Jul 30; 11(7):e1005076.

30. Heckmann BL, Green DR. LC3-associated phagocytosis at a glance. J Cell Sci. 2019 Mar 1; 132(5): jcs231472.

31. Wan J, Weiss E, Ben Mkaddem S, Mabire M, Choinier PM, Picq O, et al. LC3-associated phagocytosis protects against inflammation and liver fibrosis via immunoreceptor inhibitory signaling. Sci Transl Med. 2020 Apr 15; 12(539):eaaw8523. https://doi.org/10.1126/scitranslmed.aaw8523 PMID: 32295902

32. Inomata M, Xu S, Chandra P, Meydani SN, Takemura G, Philips JA, et al. Macrophage LC3-associated phagocytosis is an immune defense against *Streptococcus pneumoniae* that diminishes with host aging. Proc Natl Acad Sci U S A. 2020 Dec 29; 117(52):33561–9.

33. Martinez J, Almendinger J, Oberst A, Ness R, Dillon CP, Fitzgerald P, et al. Microtubule-associated protein 1 light chain 3 alpha (LC3)-associated phagocytosis is required for the efficient clearance of dead cells. Proc Natl Acad Sci U S A. 2011 Oct 18; 108(42):17396–401. https://doi.org/10.1073/pnas.1113421108 PMID: 21969579

34. Sanjuan MA, Dillon CP, Tait SWG, Moshiach S, Dorsey F, Connell S, et al. Toll-like receptor signalling in macrophages links the autophagy pathway to phagocytosis. Nature. 2007 Dec; 450(7173):1253–7. https://doi.org/10.1038/nature06421 PMID: 18097414

35. Cohen SB, Gern BH, Delahaye JL, Adams KN, Plumlee CR, Winkler JK, et al. Alveolar Macrophages Provide an Early Mycobacterium tuberculosis Niche and Initiate Dissemination. Cell Host Microbe. 2018 Sep; 24(3):439–446.e4. https://doi.org/10.1016/j.chom.2018.08.001 PMID: 30146391

36. Rothchild AC, Olson GS, Nemeth J, Amon LM, Mai D, Gold ES, et al. Alveolar macrophages generate a noncanonical NRF2-driven transcriptional response *to Mycobacterium tuberculosis* in vivo. Sci Immunol. 2019 Jul 5; 4(37):eaaw6693.

37. Vieira S, Lemos H, Grespan R, Napimoga M, Dal-Secco D, Freitas A, et al. A crucial role for TNF-a in mediating neutrophil influx induced by endogenously generated or exogenous chemokines, KC/CXCL1 and LIX/CXCL5. Br J Pharmacol. 2009; 11.

38. Bendall LJ, Bradstock KF. G-CSF: From granulopoietic stimulant to bone marrow stem cell mobilizing agent. Cytokine Growth Factor Rev. 2014 Aug; 25(4):355–67. https://doi.org/10.1016/j.cytogfr.2014.07.011 PMID: 25131807

39. Semerad CL, Liu F, Gregory AD, Stumpf K, Link DC. G-CSF Is an Essential Regulator of Neutrophil Trafficking from the Bone Marrow to the Blood. Immunity. 2002 Oct; 17(4):413–23. https://doi.org/10.1016/s1074-7613(02)00424-7 PMID: 12387736

40. Pollara G, Turner CT, Rosenheim J, Chandran A, Bell LCK, Khan A, et al. Exaggerated IL-17A activity in human in vivo recall responses discriminates active tuberculosis from latent infection and cured disease. Sci Transl Med. 2021 May 5; 13(592):eabg7673. https://doi.org/10.1126/scitranslmed.abg7673 PMID: 33952677

41. Sasaki Y, Guo YM, Goto T, Ubukawa K, Asanuma K, Kobayashi I, et al. IL-6 Generated from Human Hematopoietic Stem and Progenitor Cells through TLR4 Signaling Promotes Emergency Granulopoiesis by Regulating Transcription Factor Expression. J Immunol. 2021 Aug 2;ji2100168. https://doi.org/10.4049/jimmunol.2100168 PMID: 34341172

42. Hu S, He W, Du X, Yang J, Wen Q, Zhong XP, et al. IL-17 Production of Neutrophils Enhances Antibacteria Ability but Promotes Arthritis Development During Mycobacterium tuberculosis Infection. EBioMedicine. 2017 Sep; 23:88–99. https://doi.org/10.1016/j.ebiom.2017.08.001 PMID: 28821374

43. Fielding CA, McLoughlin RM, McLeod L, Colmont CS, Najdovska M, Grail D, et al. IL-6 Regulates Neutrophil Trafficking during Acute Inflammation via STAT3. J Immunol. 2008 Aug 1; 181(3):2189–95. https://doi.org/10.4049/jimmunol.181.3.2189 PMID: 18641358

44. Saitoh T, Akira S. Regulation of inflammasomes by autophagy. J Allergy Clin Immunol. 2016 Jul; 138 (1):28–36. https://doi.org/10.1016/j.jaci.2016.05.009 PMID: 27373323

45. Harris J, Hartman M, Roche C, Zeng SG, O'Shea A, Sharp FA, et al. Autophagy Controls IL-1β Secretion by Targeting Pro-IL-1β for Degradation. J Biol Chem. 2011 Mar; 286(11):9587–97.

46. Pang Y, Wu L, Tang C, Wang H, Wei Y. Autophagy-Inflammation Interplay During Infection: Balancing Pathogen Clearance and Host Inflammation. Front Pharmacol. 2022 Feb 22; 13:832750. https://doi.org/10.3389/fphar.2022.832750 PMID: 35273506

47. Ko JH, Yoon SO, Lee HJ, Oh JY. Rapamycin regulates macrophage activation by inhibiting NLRP3 inflammasome-p38 MAPK-NFκB pathways in autophagy- and p62-dependent manners. Oncotarget. 2017 Jun 20; 8(25):40817–31.

48. Shi CS, Shenderov K, Huang NN, Kabat J, Abu-Asab M, Fitzgerald KA, et al. Activation of autophagy by inflammatory signals limits IL-1β production by targeting ubiquitinated inflammasomes for destruction. Nat Immunol. 2012 Mar; 13(3):255–63.

49. Pyrillou K, Burzynski LC, Clarke MCH. Alternative Pathways of IL-1 Activation, and Its Role in Health and Disease. Front Immunol. 2020 Dec 18; 11:613170. https://doi.org/10.3389/fimmu.2020.613170 PMID: 33391283

50. McElvania TeKippe E, Allen IC, Hulseberg PD, Sullivan JT, McCann JR, Sandor M, et al. Granuloma Formation and Host Defense in Chronic Mycobacterium tuberculosis Infection Requires PYCARD/ASC but Not NLRP3 or Caspase-1. Tyagi AK, editor. PLoS ONE. 2010 Aug 20; 5(8):e12320. https://doi.org/10.1371/journal.pone.0012320 PMID: 20808838

51. Beckwith KS, Beckwith MS, Ullmann S, Sætra RS, Kim H, Marstad A, et al. Plasma membrane damage causes NLRP3 activation and pyroptosis during Mycobacterium tuberculosis infection. Nat Commun. 2020 Dec; 11(1):2270. https://doi.org/10.1038/s41467-020-16143-6 PMID: 32385301

52. Abdalla H, Srinivasan L, Shah S, Mayer-Barber KD, Sher A, Sutterwala FS, et al. Mycobacterium tuberculosis Infection of Dendritic Cells Leads to Partially Caspase-1/11-Independent IL-1β and IL-18 Secretion but Not to Pyroptosis. Kwaik YA, editor. PLoS ONE. 2012 Jul 24; 7(7):e40722.

53. Mayer-Barber KD, Barber DL, Shenderov K, White SD, Wilson MS, Cheever A, et al. Cutting Edge: Caspase-1 Independent IL-1β Production Is Critical for Host Resistance to *Mycobacterium tuberculosis* and Does Not Require TLR Signaling In Vivo. J Immunol. 2010 Apr 1; 184(7):3326–30.

54. Lin KM, Hu W, Troutman TD, Jennings M, Brewer T, Li X, et al. IRAK-1 bypasses priming and directly links TLRs to rapid NLRP3 inflammasome activation. Proc Natl Acad Sci U S A. 2014 Jan 14; 111 (2):775–80. https://doi.org/10.1073/pnas.1320294111 PMID: 24379360

55. Qiao Yu, Wang Peng, Qi Jianni, Zhang Lei, Gao Chengjiang. TLR-induced NF-jB activation regulates NLRP3 expression in murine macrophages. 2012; 586:1022–6.

56. Goldberg MS, Fleming SM, Palacino JJ, Cepeda C, Lam HA, Bhatnagar A, et al. Parkin-deficient Mice Exhibit Nigrostriatal Deficits but Not Loss of Dopaminergic Neurons. J Biol Chem. 2003 Oct; 278 (44):43628–35. https://doi.org/10.1074/jbc.M308947200 PMID: 12930822

57. Lazarou M, Sliter DA, Kane LA, Sarraf SA, Wang C, Burman JL, et al. The ubiquitin kinase PINK1 recruits autophagy receptors to induce mitophagy. Nature. 2015 Aug; 524(7565):309–14. https://doi.org/10.1038/nature14893 PMID: 26266977

58. Killackey SA, Philpott DJ, Girardin SE. Mitophagy pathways in health and disease. J Cell Biol. 2020 Nov 2; 219(11):e202004029. https://doi.org/10.1083/jcb.202004029 PMID: 32926082

59. Zhang W, Ren H, Xu C, Zhu C, Wu H, Liu D, et al. Hypoxic mitophagy regulates mitochondrial quality and platelet activation and determines severity of I/R heart injury. elife. 2016 Dec 20; 5:e21407. https://doi.org/10.7554/eLife.21407 PMID: 27995894

60. Wang SH, Martin SM, Harris PS, Knudson CM. Caspase Inhibition Blocks Cell Death and Enhances Mitophagy but Fails to Promote T-Cell Lymphoma. Chandra D, editor. PLoS ONE. 2011 May 17; 6(5): e19786. https://doi.org/10.1371/journal.pone.0019786 PMID: 21611191

61. Nguyen TN, Padman BS, Lazarou M. Deciphering the Molecular Signals of PINK1/Parkin Mitophagy. Trends Cell Biol. 2016 Oct; 26(10):733–44. https://doi.org/10.1016/j.tcb.2016.05.008 PMID: 27291334

62. Harris J, Deen N, Zamani S, Hasnat MA. Mitophagy and the release of inflammatory cytokines. Mitochondrion. 2018 Jul; 41:2–8. https://doi.org/10.1016/j.mito.2017.10.009 PMID: 29107116

63. Song Y, Zhou Y, Zhou X. The role of mitophagy in innate immune responses triggered by mitochondrial stress. Cell Commun Signal. 2020 Dec; 18(1):186. https://doi.org/10.1186/s12964-020-00659-x PMID: 33239048

64. Griffin GK, Newton G, Tarrio ML, Bu DV, Maganto-Garcia E, Azcutia V, et al. IL-17 and TNF-α Sustain Neutrophil Recruitment during Inflammation through Synergistic Effects on Endothelial Activation. J Immunol. 2012 Jun 15; 188(12):6287–99.

65. Roussel L, Houle F, Chan C, Yao Y, Bérubé J, Olivenstein R, et al. IL-17 Promotes p38 MAPK-Dependent Endothelial Activation Enhancing Neutrophil Recruitment to Sites of Inflammation. J Immunol. 2010 Apr 15; 184(8):4531–7. https://doi.org/10.4049/jimmunol.0903162 PMID: 20228195

66. Halwani R, Al-Muhsen S, Hamid Q. T Helper 17 Cells in Airway Diseases. Chest. 2013 Feb; 143 (2):494–501.

67. Ding WX, Jaeschke H. Autophagy in macrophages regulates the inflammasome and protects against liver injury. J Hepatol. 2016 Jan; 64(1):16–8. https://doi.org/10.1016/j.jhep.2015.10.003 PMID: 26456339

68. Bussi C, Peralta Ramos JM, Arroyo DS, Gaviglio EA, Gallea JI, Wang JM, et al. Autophagy down regulates pro-inflammatory mediators in BV2 microglial cells and rescues both LPS and alpha-synuclein induced neuronal cell death. Sci Rep. 2017 Mar 3; 7(1):43153. https://doi.org/10.1038/srep43153 PMID: 28256519

69. Peng X, Wang Y, Li H, Fan J, Shen J, Yu X, et al. ATG5-mediated autophagy suppresses NF-κB signaling to limit epithelial inflammatory response to kidney injury. Cell Death Dis. 2019 Mar 15; 10(4):253.

70. Chang CP, Su YC, Hu CW, Lei HY. TLR2-dependent selective autophagy regulates NF-κB lysosomal degradation in hepatoma-derived M2 macrophage differentiation. Cell Death Differ. 2013 Mar; 20 (3):515–23.

71. Liu K, Zhang L, Zhao Q, Zhao Z, Zhi F, Qin Y, et al. SKP2 attenuates NF-κB signaling by mediating IKKβ degradation through autophagy. Su B, editor. J Mol Cell Biol. 2018 Jun 1; 10(3):205–215.

72. Yang Q, Liu TT, Lin H, Zhang M, Wei J, Luo WW, et al. TRIM32-TAX1BP1-dependent selective autophagic degradation of TRIF negatively regulates TLR3/4-mediated innate immune responses. Philpott DJ, editor. PLoS Pathog. 2017 Sep 12; 13(9):e1006600. https://doi.org/10.1371/journal.ppat.1006600 PMID: 28898289

73. Lim J, Park H, Heisler J, Maculins T, Roose-Girma M, Xu M, et al. Autophagy regulates inflammatory programmed cell death via turnover of RHIM-domain proteins. elife. 2019 Jul 9; 8:e44452. https://doi.org/10.7554/eLife.44452 PMID: 31287416

74. Bock FJ, Riley JS. When cell death goes wrong: inflammatory outcomes of failed apoptosis and mitotic cell death. Cell Death Differ. 2023 Feb; 30(2):293–303. https://doi.org/10.1038/s41418-022-01082-0 PMID: 36376381

75. Tang D, Kang R, Coyne CB, Zeh HJ, Lotze MT. PAMPs and DAMPs: signal 0s that spur autophagy and immunity. Immunol Rev. 2012 Sep; 249(1):158–75. https://doi.org/10.1111/j.1600-065X.2012.01146.x PMID: 22889221

76. Zhao X, Khan N, Gan H, Tzelepis F, Nishimura T, Park SY, et al. Bcl-xL mediates RIPK3-dependent necrosis in M. tuberculosis-infected macrophages. Mucosal Immunol. 2017; 10(6):1553–1568. https://doi.org/10.1038/mi.2017.12 PMID: 28401933

77. Yousefi S, Perozzo R, Schmid I, Ziemiecki A, Schaffner T, Scapozza L, et al. Calpain-mediated cleavage of Atg5 switches autophagy to apoptosis. Nat Cell Biol. 2006 Oct; 8(10):1124–32. https://doi.org/10.1038/ncb1482 PMID: 16998475

78. Mázló A, Jenei V, Burai S, Molnár T, Bácsi A, Koncz G. Types of necroinflammation, the effect of cell death modalities on sterile inflammation. Cell Death Dis. 2022 May 2; 13(5):423. https://doi.org/10.1038/s41419-022-04883-w PMID: 35501340

79. Doran AC, Yurdagul A, Tabas I. Efferocytosis in health and disease. Nat Rev Immunol. 2020 Apr; 20 (4):254–67. https://doi.org/10.1038/s41577-019-0240-6 PMID: 31822793

80. Asare PF, Roscioli E, Hurtado PR, Tran HB, Mah CY, Hodge S. LC3-Associated Phagocytosis (LAP): A Potentially Influential Mediator of Efferocytosis-Related Tumor Progression and Aggressiveness. Front Oncol. 2020 Aug 5; 10:1298. https://doi.org/10.3389/fonc.2020.01298 PMID: 32850405

81. Moretti J, Roy S, Bozec D, Martinez J, Chapman JR, Ueberheide B, et al. STING Senses Microbial Viability to Orchestrate Stress-Mediated Autophagy of the Endoplasmic Reticulum. Cell. 2017; 171 (4):809–823.e13. https://doi.org/10.1016/j.cell.2017.09.034 PMID: 29056340

82. Chipurupalli S, Samavedam U, Robinson N. Crosstalk Between ER Stress, Autophagy and Inflammation. Front Med. 2021; 5(8):758311. https://doi.org/10.3389/fmed.2021.758311 PMID: 34805224

83. Niven J, Madelon N, Page N, Caruso A, Harlé G, Lemeille S, et al. Macroautophagy in Dendritic Cells Controls the Homeostasis and Stability of Regulatory T Cells. Cell Rep. 2019 Jul; 28(1):21–29.e6. https://doi.org/10.1016/j.celrep.2019.05.110 PMID: 31269441

84. Peral de Castro C, Jones SA, Ní Cheallaigh C, Hearnden CA, Williams L, Winter J, et al. Autophagy Regulates IL-23 Secretion and Innate T Cell Responses through Effects on IL-1 Secretion. J Immunol. 2012 Oct 15; 189(8):4144–53.

85. Cho ML, Kang JW, Moon YM, Nam HJ, Jhun JY, Heo SB, et al. STAT3 and NF-κB Signal Pathway Is Required for IL-23-Mediated IL-17 Production in Spontaneous Arthritis Animal Model IL-1 Receptor Antagonist-Deficient Mice. J Immunol. 2006 May 1; 176(9):5652–61.

86. Sutton C, Brereton C, Keogh B, Mills KHG, Lavelle EC. A crucial role for interleukin (IL)-1 in the induction of IL-17–producing T cells that mediate autoimmune encephalomyelitis. J Exp Med. 2006 Jul 10; 203(7):1685–91. https://doi.org/10.1084/jem.20060285 PMID: 16818675

87. Gawriluk TR, Hale AN, Flaws JA, Dillon CP, Green DR, Rucker EB. Autophagy is a cell survival program for female germ cells in the murine ovary. Reproduction. 2011 Jun; 141(6):759–65. https://doi.org/10.1530/REP-10-0489 PMID: 21464117

88. Hara T, Nakamura K, Matsui M, Yamamoto A, Nakahara Y, Suzuki-Migishima R, et al. Suppression of basal autophagy in neural cells causes neurodegenerative disease in mice. Nature. 2006 Jun; 441 (7095):885–9. https://doi.org/10.1038/nature04724 PMID: 16625204

89. Hwang S, Maloney NS, Bruinsma MW, Goel G, Duan E, Zhang L, et al. Nondegradative Role of Atg5-Atg12/ Atg16L1 Autophagy Protein Complex in Antiviral Activity of Interferon Gamma. Cell Host Microbe. 2012 Apr; 11(4):397–409. https://doi.org/10.1016/j.chom.2012.03.002 PMID: 22520467

90. Martinez J, Malireddi RKS, Lu Q, Cunha LD, Pelletier S, Gingras S, et al. Molecular characterization of LC3-associated phagocytosis reveals distinct roles for Rubicon, NOX2 and autophagy proteins. Nat Cell Biol. 2015 Jul; 17(7):893–906. https://doi.org/10.1038/ncb3192 PMID: 26098576

91. Kitada T, Pisani A, Porter DR, Yamaguchi H, Tscherter A, Martella G, et al. Impaired dopamine release and synaptic plasticity in the striatum of *PINK1* -deficient mice. Proc Natl Acad Sci U S A. 2007 Jul 3; 104(27):11441–6.

92. Huynh JP, Lin CC, Kimmey JM, Jarjour NN, Schwarzkopf EA, Bradstreet TR, et al. Bhlhe40 is an essential repressor of IL-10 during Mycobacterium tuberculosis infection. J Exp Med. 2018 Jul 2; 215 (7):1823–38. https://doi.org/10.1084/jem.20171704 PMID: 29773644

93. Domingo-Gonzalez R, Das S, Griffiths KL, Ahmed M, Bambouskova M, Gopal R, et al. Interleukin-17 limits hypoxia-inducible factor 1α and development of hypoxic granulomas during tuberculosis. JCI Insight. 2017 Oct 5; 2(19):e92973.